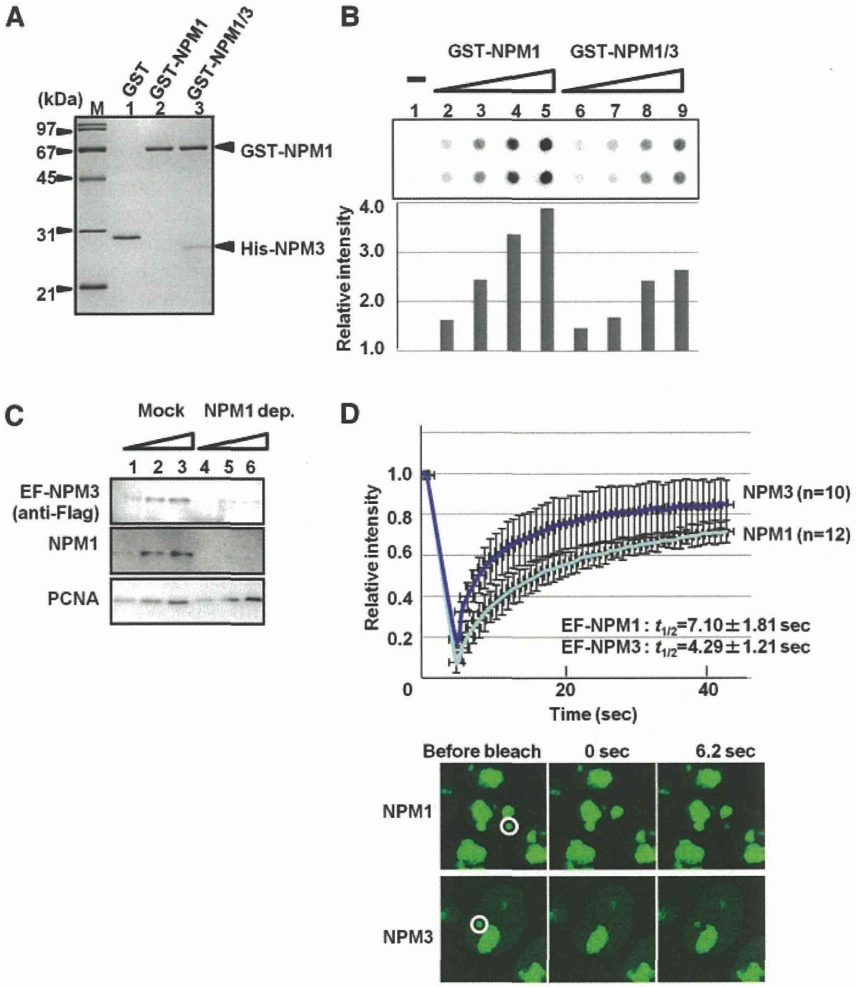

Figure 8. Effects of NPM3 incorporation into the NPM1 pentamer on the NPM1 functions in somatic cells. (**A**) Purified GST–NPM1/His–NPM3 oligomer. GST–NPM1 was first purified and denatured in the absence or presence of three times molar excess of His–NPM3, the mixtures were dialyzed to refold the proteins and the excess His–NPM3 was removed by purification of the proteins with glutathione sepharose. GST, GST–NPM1 and GST–NPM1/His–NPM3 (lanes 1–3, respectively, 200 ng of GST proteins) were separated on 12.5% SDS–PAGE and visualized with CBB staining. (**B**) RNA-binding activity of the NPM1–NPM3 complex. Increasing amounts of GST–NPM1 and GST–NPM1/His–NPM3 were mixed with ^{32}P-labeled total RNA purified from HeLa cells. The mixture was filtrated through nitrocellulose membrane. The membrane was extensively washed and the radio-active RNA retained on the membrane was detected by BAS2500 image analyzing system (top panel). Experiments were performed with doublet and the average radioactivity of the retained RNA is graphically shown at the bottom. The radio-active RNA incubated in the absence of NPM proteins (lane 1) retained on the membrane was set as 1.0 and relative amounts of retained RNA were measured. Two independent experiments demonstrated similar results. (**C**) Depletion of NPM1 from the extracts. NPM1 was immune-depleted from the extracts prepared from HeLa cells stably expressing EF–NPM3 using an anti-NPM1 antibody. Increasing amounts (1, 3 and 10 μg of proteins) of mock- and NPM1-depleted extracts (lanes 1–3 and 4–6, respectively) were separated by SDS–PAGE and analyzed by western blotting with anti-Flag, anti-NPM1 and anti-PCNA antibodies. (**D**) FRAP analysis of NPM1 and NPM3. HeLa cells stably expressing either EF–NPM1 or EF–NPM3 were grown on the glass-base dishes. FRAP analyses were performed as described in 'Materials and Methods' section. Small nucleoli as shown by white circle in the left panels were breached by a 488-nm laser and the fluorescent recovery at the bleached nucleoli was measured every 0.5 s. The fluorescence at the bleached area relative to the initial fluorescence (1.0) was calculated and plotted as a function of time. The data are represented as mean values ± SD from 12 and 10 experiments for NPM1 and NPM3, respectively. The $t_{1/2}$ of fluorescence recovery (7.10 and 4.29 s for NPM1 and NPM3, respectively) was estimated by curve fitting as described in 'Materials and Methods' section. Typical FRAP images of EF–NPM1 and EF–NPM3 before bleaching, and 0 and 6.2 s after bleaching are shown at the bottom.

proteins can potentially remodel sperm chromatin. Furthermore, we also found that NPM3 enhanced the dynamics of NPM1 in somatic growing cell nuclei (Figure 8).

Oligomer formation by human NPM proteins

Unlike NPM1 and NPM2, NPM3 did not form stable homopentamers/decamers in solution (Figure 2). The NPM3 crystal structure has not been reported until date; therefore, it is difficult to understand why NPM3 cannot form a homopentamer. The trypsin digestion assay suggested that NPM3 forms a compact typical NPM core structure to form dimers or trimers in solution (Figures 2 and 6). NPM3 has conserved sequences such as the AKDE sequence and K-loop required for pentamer–pentamer interaction (Figure 2D) (10,11). Thus, dimer

or trimer formation could be mediated by these sequences. However, given that the expression level of NPM3 was significantly lower than that of NPM1 in HeLa cells and mouse oocytes (Figure 1D and F) and NPM3 was efficiently depleted with NPM1 from cell extracts (Figure 8C), NPM3 mainly functions with NPM1 in cells. Crosslinking experiments and BN–PAGE data (Figure 2) suggested that NPM1 and NPM3 preferentially form a decamer consisting of two NPM1:NPM3 (4:1) pentamers. If a NPM3 molecule can form contacts with two NPM1 molecules, a NPM1–NPM3 (3:2) complex should be formed in addition to the (4:1) complex. However, we could not detect a clear band corresponding to the NPM1–NPM3 (3:2) complex by BN–PAGE (Figure 6B), suggesting that only one monomer–monomer interaction surface is likely to be active in NPM3. In addition, gel filtration analysis revealed that the NPM1–NPM3 complex was less stable than NPM1 alone (Figure 6D).

Nucleic acid-binding activity of human NPM2

We found that human NPM2 has potential DNA and RNA-binding activities (Figure 4B and data not shown) that are regulated by phosphorylation with mitotic extracts (Figure 4). In germinal vesicles (GV), the phosphorylation status of mouse NPM2 was found to be significantly lower than that of NPM2 in MII stage eggs (31). NPM2 is localized in the nucleoplasm and also in the nucleolus-like bodies (NLB) in GVs, but it is also distributed throughout the cell upon entry into the MII stage (5,27,31). This localization change is extremely similar to that found with NPM1 in growing somatic cells. NPM1 is mainly localized in the interphase nucleolus but becomes distributed throughout the cell during mitosis when the RNA-binding activity of NPM1 is suppressed by phosphorylation with cyclin B/cdc2 kinase (23). A NPM1 mutant mimicking mitotic phosphorylation status cannot stably localize in the nucleolus, even in interphase cells (32). Based on the relationship between the RNA-binding activity and nucleolar localization of NPM1, it is strongly suggested that NPM2 localization in NLBs is regulated by its nucleic acid-binding activity. The C-terminal basic clusters of mouse NPM2 were shown to be necessary for NLB localization in and formation of GVs (27). In addition, NPM2 possesses nuclear remodeling activity (3,4). Thus, we propose that the NLB localization of NPM2 in GVs is important for restricting any unfavorable remodeling of maternal chromatin.

Sperm chromatin remodeling by human NPM proteins

NPM1 and the NPM1–NPM3 complex efficiently mediated sperm chromatin decondensation and nucleosome assembly, whereas NPM2 activity was lower than those of NPM1 and the NPM1–NPM3 complex. Mouse and human NPM2 proteins do not possess the typical 'A1 tract', an acidic amino acid cluster, in the core domain, which is conserved in most NPM family proteins (Figure 2D). The A1 tract of *Xenopus* nucleoplasmin/NPM2 was shown to be crucial for sperm chromatin decondensation activity (33). In addition, the human NPM2 core domain alone did not efficiently bind to histones (9). This could be the reason why human NPM2 did not show efficient sperm chromatin remodeling activity. However, it is reasonable to speculate that NPM2 has sperm chromatin decondensation activity because sperm chromatin decondensation was reduced in NPM2 knock out mouse eggs (5,27), and the expression level of NPM2 was higher than those of NPM1 and NPM3 (Figure 1F). The N-terminal flexible region and the C-terminal basic region of nucleoplasmin (*Xenopus* NPM2) are phosphorylated in *Xenopus* eggs, and the phosphorylation of these two tail domains was found to be necessary for efficient sperm chromatin remodeling (30,34). Potential phosphorylation sites in the N-terminal tail domain and the C-terminal basic region are conserved in human NPM2 and phosphomimetic mutation at these sites significantly increased the sperm chromatin remodeling activity of NPM2 (Figure 4D and E). Thus, it is likely that the NPM2 activity is regulated by phosphorylation during oogenesis and after fertilization. Since the activity of phosphomimetic NPM2 mutants was lower than that of NPM1, it is possible that additional phosphorylation sites are involved in the stimulation of NPM2 activity.

Sperm chromatin decondensation occurs in NPM2 knockout mice eggs (5,27). It is therefore clear that additional factors are necessary for sperm chromatin remodeling. As shown in this study, NPM1 and NPM3 are good candidate sperm chromatin decondensation factors in fertilized eggs. Furthermore, NAP/SET family proteins (Nap1-like proteins and SET/TAF-I) are ubiquitously expressed and have potential sperm chromatin decondensation activity (21,35). Moreover, the histone chaperone HIRA and the chromatin remodeling protein CHD1 cooperatively mediate nucleosome assembly with histone H3.3 in the paternal genome (36,37). Given that sperm chromatin decondensation depends on the concentration of decondensation factor(s), the determination of the stoichiometry between these candidate factors should help elucidate the mechanism of this process.

NPM3 function in growing somatic cells

Our results clearly indicate that NPM3 can mediate sperm chromatin remodeling when included in a pentamer with NPM1 (Figure 7). Moreover, we found that NPM3 regulates NPM1 mobility in growing somatic cells (Figure 8). However, the exact cellular function of NPM3 has not been clarified. Transient expression of NPM3 inhibits the ribosome biogenesis function of NPM1 in a transformed monkey cell line (26). These results suggest that NPM3 is a negative regulator of cell growth, possibly through the inhibition of NPM1 function. In contrast, endogenous NPM3 is highly expressed in mouse ES cells, where the expression level is decreased after differentiation, and NPM3 overexpression in ES cells increases cell growth (25). We also found that NPM3 expression in normal human fibroblast cells is much lower than that found in cancer-derived cell lines, including HeLa and 293T cells (data not shown). Therefore, it seems likely that NPM3 expression is associated with cell growth rate. As shown in Figure 8, NPM1 mobility appeared to

be increased by complex formation with NPM3. Nucleo-cytoplasmic shuttling of NPM1 was shown to contribute to the export of ribosome subunits (38–40), thereby decreasing cell growth. These results suggest that the nucleo-cytoplasmic shuttling of NPM1 is important for positive cell growth. In this regard, NPM3 may have a growth-associated function.

Finally, it should be mentioned that the NPM1–NPM3 complex functions as an active histone chaperone (Figure 6). NPM3 incorporation into the NPM1 oligomer increases NPM1 retention time in the nucleoplasm, and it is possible that the NPM1–NPM3 complex is involved in the regulation of chromatin structure at the specific gene loci driven by RNA polymerase II. NPM1 is associated with a variety of RNA polymerase II-regulated genes (41). Therefore, it would be interesting to test whether NPM1 and NPM3 cooperatively regulate the gene expression profile in somatic growing cells.

ACKNOWLEDGEMENTS

The authors thank Drs Alain Verreault (University of Montreal) and Martin Matzuk (Baylor College of Medicine) for reagents, and Keijiro Kato for his technical assistance. The authors also thank Dr Kensaku Murano (University of Tsukuba) for his help to prepare mouse sperms and MII oocytes.

FUNDING

PRESTO from Japan Science and Technology Agency (JST); Special Coordination Funds for Promoting Science and Technology from JST; Grants–in–aid for Scientific Research from the Ministry of Education, Culture, Sports, Science and Technology of Japan. Funding for open access charge: Special Coordination Funds for Promoting Science and Technology from JST.

Conflict of interest statement. None declared.

REFERENCES

1. Laskey,R.A., Honda,B.M., Mills,A.D. and Finch,J.T. (1978) Nucleosomes are assembled by an acidic protein which binds histones and transfers them to DNA. *Nature*, **275**, 416–420.
2. Philpott,A. and Leno,G.H. (1992) Nucleoplasmin remodels sperm chromatin in Xenopus egg extracts. *Cell*, **69**, 759–767.
3. Tamada,H., Van Thuan,N., Reed,P., Nelson,D., Katoku-Kikyo,N., Wudel,J., Wakayama,T. and Kikyo,N. (2006) Chromatin decondensation and nuclear reprogramming by nucleoplasmin. *Mol. Cell Biol.*, **26**, 1259–1271.
4. Sylvestre,E.L., Pennetier,S., Bureau,M., Robert,C. and Sirard,M.A. (2010) Investigating the potential of genes preferentially expressed in oocyte to induce chromatin remodeling in somatic cells. *Cell Reprogram*, **12**, 519–528.
5. Burns,K.H., Viveiros,M.M., Ren,Y., Wang,P., DeMayo,F.J., Frail,D.E., Eppig,J.J. and Matzuk,M.M. (2003) Roles of NPM2 in chromatin and nucleolar organization in oocytes and embryos. *Science*, **300**, 633–636.
6. Okuwaki,M., Matsumoto,K., Tsujimoto,M. and Nagata,K. (2001) Function of nucleophosmin/B23, a nucleolar acidic protein, as a histone chaperone. *FEBS Lett.*, **506**, 272–276.
7. McLay,D.W. and Clarke,H.J. (2003) Remodelling the paternal chromatin at fertilization in mammals. *Reproduction*, **125**, 625–633.
8. Akey,C.W. and Luger,K. (2003) Histone chaperones and nucleosome assembly. *Curr. Opin. Struct. Biol.*, **13**, 6–14.
9. Platonova,O., Akey,I.V., Head,J.F. and Akey,C.W. (2011) Crystal structure and function of human nucleoplasmin (npm2): a histone chaperone in oocytes and embryos. *Biochemistry*, **50**, 8078–8089.
10. Dutta,S., Akey,I.V., Dingwall,C., Hartman,K.L., Laue,T., Nolte,R.T., Head,J.F. and Akey,C.W. (2001) The crystal structure of nucleoplasmin-core: implications for histone binding and nucleosome assembly. *Mol. Cell*, **8**, 841–853.
11. Namboodiri,V.M., Akey,I.V., Schmidt-Zachmann,M.S., Head,J.F. and Akey,C.W. (2004) The structure and function of Xenopus NO38-core, a histone chaperone in the nucleolus. *Structure*, **12**, 2149–2160.
12. Namboodiri,V.M., Dutta,S., Akey,I.V., Head,J.F. and Akey,C.W. (2003) The crystal structure of Drosophila NLP-core provides insight into pentamer formation and histone binding. *Structure*, **11**, 175–186.
13. Lee,H.H., Kim,H.S., Kang,J.Y., Lee,B.I., Ha,J.Y., Yoon,H.J., Lim,S.O., Jung,G. and Suh,S.W. (2007) Crystal structure of human nucleophosmin-core reveals plasticity of the pentamer-pentamer interface. *Proteins*, **69**, 672–678.
14. Frehlick,L.J., Eirín-López,J.M. and Ausió,J. (2007) New insights into the nucleophosmin/nucleoplasmin family of nuclear chaperones. *Bioessays*, **29**, 49–59.
15. Wang,D., Umekawa,H. and Olson,M.O. (1993) Expression and subcellular locations of two forms of nucleolar protein B23 in rat tissues and cells. *Cell Mol. Biol. Res.*, **39**, 33–42.
16. Haruki,H., Okuwaki,M., Miyagishi,M., Taira,K. and Nagata,K. (2006) Involvement of template-activating factor I/SET in transcription of adenovirus early genes as a positive-acting factor. *J. Virol.*, **80**, 794–801.
17. Matsumoto,K., Nagata,K., Ui,M. and Hanaoka,F. (1993) Template activating factor I, a novel host factor required to stimulate the adenovirus core DNA replication. *J. Biol. Chem.*, **268**, 10582–10587.
18. Okuwaki,M., Iwamatsu,A., Tsujimoto,M. and Nagata,K. (2001) Identification of nucleophosmin/B23, an acidic nucleolar protein, as a stimulatory factor for in vitro replication of adenovirus DNA complexed with viral basic core proteins. *J. Mol. Biol.*, **311**, 41–55.
19. Samad,M.A., Okuwaki,M., Haruki,H. and Nagata,K. (2007) Physical and functional interaction between a nucleolar protein nucleophosmin/B23 and adenovirus basic core proteins. *FEBS Lett.*, **581**, 3283–3288.
20. Sung,M.T., Cao,T.M., Coleman,R.T. and Budelier,K.A. (1983) Gene and protein sequences of adenovirus protein VII, a hybrid basic chromosomal protein. *Proc. Natl Acad. Sci. USA*, **80**, 2902–2906.
21. Matsumoto,K., Nagata,K., Miyaji-Yamaguchi,M., Kikuchi,A. and Tsujimoto,M. (1999) Sperm chromatin decondensation by template activating factor I through direct interaction with basic proteins. *Mol. Cell Biol.*, **19**, 6940–6952.
22. Hisaoka,M., Ueshima,S., Murano,K., Nagata,K. and Okuwaki,M. (2010) Regulation of nucleolar chromatin by B23/nucleophosmin jointly depends upon its RNA binding activity and transcription factor UBF. *Mol. Cell Biol.*, **30**, 4952–4964.
23. Okuwaki,M., Tsujimoto,M. and Nagata,K. (2002) The RNA binding activity of a ribosome biogenesis factor, nucleophosmin/B23, is modulated by phosphorylation with a cell cycle-dependent kinase and by association with its subtype. *Mol. Biol. Cell.*, **13**, 2016–2030.
24. Okuwaki,M., Kato,K., Shimahara,H., Tate,S. and Nagata,K. (2005) Assembly and disassembly of nucleosome core particles containing histone variants by human nucleosome assembly protein I. *Mol. Cell Biol.*, **25**, 10639–10651.
25. Motoi,N., Suzuki,K., Hirota,R., Johnson,P., Oofusa,K., Kikuchi,Y. and Yoshizato,K. (2008) Identification and characterization of nucleoplasmin 3 as a histone-binding protein in embryonic stem cells. *Dev. Growth Differ.*, **50**, 307–320.
26. Huang,N., Negi,S., Szebeni,A. and Olson,M.O. (2005) Protein NPM3 interacts with the multifunctional nucleolar protein

B23/nucleophosmin and inhibits ribosome biogenesis. *J. Biol. Chem.*, **280**, 5496–5502.
27. Inoue,A., Ogushi,S., Saitou,M., Suzuki,M.G. and Aoki,F. (2011) Involvement of mouse nucleoplasmin 2 in the decondensation of sperm chromatin after fertilization. *Biol. Reprod.*, **85**, 70–77.
28. Wittig,I., Braun,H.P. and Schagger,H. (2006) Blue native PAGE. *Nat. Protoc.*, **1**, 418–428.
29. Gadad,S.S., Shandilya,J., Kishore,A.H. and Kundu,T.K. (2010) NPM3, a member of the nucleophosmin/nucleoplasmin family, enhances activator-dependent transcription. *Biochemistry*, **49**, 1355–1357.
30. Bañuelos,S., Omaetxebarria,M.J., Ramos,I., Larsen,M.R., Arregi,I., Jensen,O.N., Arizmendi,J.M., Prado,A. and Muga,A. (2007) Phosphorylation of both nucleoplasmin domains is required for activation of its chromatin decondensation activity. *J. Biol. Chem.*, **282**, 21213–21221.
31. Vitale,A.M., Calvert,M.E., Mallavarapu,M., Yurttas,P., Perlin,J., Herr,J. and Coonrod,S. (2007) Proteomic profiling of murine oocyte maturation. *Mol. Reprod. Dev.*, **74**, 608–616.
32. Negi,S.S. and Olson,M.O. (2006) Effects of interphase and mitotic phosphorylation on the mobility and location of nucleolar protein B23. *J. Cell Sci.*, **119**, 3676–3685.
33. Salvany,L., Chiva,M., Arnan,C., Ausió,J., Subirana,J.A. and Saperas,N. (2004) Mutation of the small acidic tract A1 drastically reduces nucleoplasmin activity. *FEBS Lett.*, **576**, 353–357.
34. Leno,G.H., Mills,A.D., Philpott,A. and Laskey,R.A. (1996) Hyperphosphorylation of nucleoplasmin facilitates Xenopus sperm decondensation at fertilization. *J. Biol. Chem.*, **271**, 7253–7256.
35. Ito,T., Tyler,J.K., Bulger,M., Kobayashi,R. and Kadonaga,J.T. (1996) ATP-facilitated chromatin assembly with a nucleoplasmin-like protein from Drosophila melanogaster. *J. Biol. Chem.*, **271**, 25041–25048.
36. Loppin,B., Bonnefoy,E., Anselme,C., Laurençon,A., Karr,T.L. and Couble,P. (2005) The histone H3.3 chaperone HIRA is essential for chromatin assembly in the male pronucleus. *Nature*, **437**, 1386–1390.
37. Konev,A.Y., Tribus,M., Park,S.Y., Podhraski,V., Lim,C.Y., Emelyanov,A.V., Vershilova,E., Pirrotta,V., Kadonaga,J.T., Lusser,A. *et al.* (2007) CHD1 motor protein is required for deposition of histone variant H3.3 into chromatin in vivo. *Science*, **317**, 1087–1090.
38. Maggi,L.B. Jr, Kuchenruether,M., Dadey,D.Y., Schwope,R.M., Grisendi,S., Townsend,R.R., Pandolfi,P.P. and Weber,J.D. (2008) Nucleophosmin serves as a rate-limiting nuclear export chaperone for the Mammalian ribosome. *Mol. Cell Biol.*, **28**, 7050–7065.
39. Yu,Y., Maggi,L.B. Jr, Brady,S.N., Apicelli,A.J., Dai,M.S., Lu,H. and Weber,J.D. (2006) Nucleophosmin is essential for ribosomal protein L5 nuclear export. *Mol. Cell Biol.*, **26**, 3798–3809.
40. Brady,S.N., Yu,Y., Maggi,L.B. Jr and Weber,J.D. (2004) ARF impedes NPM/B23 shuttling in an Mdm2-sensitive tumor suppressor pathway. *Mol. Cell Biol.*, **24**, 9327–9338.
41. Shandilya,J., Swaminathan,V., Gadad,S.S., Choudhari,R., Kodaganur,G.S. and Kundu,T.K. (2009) Acetylated NPM1 localizes in the nucleoplasm and regulates transcriptional activation of genes implicated in oral cancer manifestation. *Mol. Cell Biol.*, **29**, 5115–5127.

Journal of General Virology (2012), **93**, 1328–1338 DOI 10.1099/vir.0.036665-0

B23/nucleophosmin is involved in regulation of adenovirus chromatin structure at late infection stages, but not in virus replication and transcription

Mohammad Abdus Samad,[1,2]† Tetsuro Komatsu,[1]† Mitsuru Okuwaki[1,3] and Kyosuke Nagata[1]

Correspondence
Kyosuke Nagata
knagata@md.tsukuba.ac.jp

[1]Graduate School of Comprehensive Human Sciences and Faculty of Medicine, University of Tsukuba, 1-1-1 Tennohdai, Tsukuba 305-8575, Japan

[2]Department of Applied Nutrition and Food Technology, Faculty of Applied Science and Technology, Islamic University, Kushtia, Bangladesh

[3]Initiatives for the Promotion of Young Scientists' Independent Research, University of Tsukuba, 1-1-1 Tennohdai, Tsukuba 305-8577, Japan

B23/nucleophosmin has been identified *in vitro* as a stimulatory factor for replication of adenovirus DNA complexed with viral basic core proteins. In the present study, the *in vivo* function of B23 in the adenovirus life cycle was studied. It was found that both the expression of a decoy mutant derived from adenovirus core protein V that tightly associates with B23 and small interfering RNA-mediated depletion of B23 impeded the production of progeny virions. However, B23 depletion did not significantly affect the replication and transcription of the virus genome. Chromatin immunoprecipitation analyses revealed that B23 depletion significantly increased the association of viral DNA with viral core proteins and cellular histones. These results suggest that B23 is involved in the regulation of association and/or dissociation of core proteins and cellular histones with the virus genome. In addition, these results suggest that proper viral chromatin assembly, regulated in part by B23, is crucial for the maturation of infectious virus particles.

Received 21 July 2011
Accepted 12 February 2012

INTRODUCTION

Adenovirus is an icosahedral particle with a linear dsDNA of approximately 36 000 bp. The linear DNA is linked covalently to virus-encoded terminal proteins and condensed with the viral basic proteins Mu, VII and V, thus forming a chromatin-like structure termed adenoviral core/chromatin (Anderson *et al.*, 1989; Black & Center, 1979; Chatterjee *et al.*, 1985). Protein VII, a 19 kDa basic protein, is the major component of the adenoviral core and is most tightly associated with the genome (Sung *et al.*, 1983). Protein V associates loosely with the viral DNA and forms an outer shell around the core to link it to the capsid through a dimer of polypeptide VI (Brown *et al.*, 1975; Chatterjee *et al.*, 1985; Fedor & Daniell, 1983). The virus genome is thought to be packed around the hexamer of core protein VII, and each unit of the viral DNA–VII hexamer complex is bridged by core protein V (Déry *et al.*, 1985; Sung *et al.*, 1977).

†These authors contributed equally to this work.

Supplementary methods and two supplementary figures are available with the online version of this paper.

Infecting adenovirus particles are disassembled in the cytoplasm in a stepwise manner after penetration through endocytosis, and the viral core enters the nucleus through nuclear pore complexes (Greber *et al.*, 1996; Martin-Fernandez *et al.*, 2004; Nakano *et al.*, 2000; Trotman *et al.*, 2001). During entry of the virus genome into the nucleus, core protein V seems to become dissociated from the viral chromatin. Thus, viral DNA associated with core protein VII functions as a template for viral early gene transcription and DNA replication in the infected cell nucleus (Chatterjee *et al.*, 1986; Haruki *et al.*, 2006; Xue *et al.*, 2005). However, it has been reported that core proteins function as a repressor for transcription and replication *in vitro* (Johnson *et al.*, 2004; Matsumoto *et al.*, 1995; Nakanishi *et al.*, 1986). Therefore, it is suggested that core proteins are either released or remodelled after entry into the host nucleus (Chen *et al.*, 2007; Matsumoto *et al.*, 1993, 1995; Spector, 2007). Histones may associate with the incoming viral DNA (Sergeant *et al.*, 1979; Tate & Philipson, 1979). Recently, it has been shown that, as well as protein VII, cellular histones are also functional components of viral chromatin in the early phases of infection (Komatsu *et al.*, 2011). During the late stages of infection,

the precursor of core protein VII (pre-VII) and core protein V are synthesized at high levels concomitant with viral DNA synthesis, assembled onto newly replicated DNA and incorporated into immature virions (Daniell *et al.*, 1981). Newly replicated viral DNA may associate with cellular histones (Déry *et al.*, 1985). However, mature adenovirus particles do not contain cellular histones. It is still largely unknown how only the virus genome associated with viral core proteins is selectively incorporated into virions. It is also unknown which cellular factors are involved in this process.

Previously, we identified host factors termed template-activating factors (TAF)-I, -II and -III from uninfected HeLa cell extracts that remodelled the adenoviral core structure and stimulated replication and transcription from the core (Matsumoto *et al.*, 1993, 1995; Okuwaki *et al.*, 2001a). Recently, we have shown that TAF-I remodels the core structure by forming a ternary complex with adenoviral DNA–core protein VII complexes and plays an important role in the early stages of the adenovirus infection cycle (Gyurcsik *et al.*, 2006; Haruki *et al.*, 2003, 2006; Komatsu *et al.*, 2011). TAF-II is identical to nucleosome assembly protein 1 (NAP-1), a structural and functional homologue of TAF-I (Kawase *et al.*, 1996; Nagata *et al.*, 1995). The major component of TAF-III was found to be B23/nucleophosmin (Okuwaki *et al.*, 2001a).

B23/nucleophosmin is an abundant ubiquitously expressed cellular protein that modulates diverse molecular functions such as ribosome biogenesis (Hingorani *et al.*, 2000; Savkur & Olson, 1998), centrosome duplication (Okuda *et al.*, 2000), chromatin assembly/disassembly (Okuwaki *et al.*, 2001b, 2005) and nucleo-cytoplasmic trafficking (Adachi *et al.*, 1993; Yu *et al.*, 2006). Two splicing variants of B23, B23.1 and B23.2, which differ only in their C-terminal regions, are expressed in a variety of growing cells. Both B23.1 and B23.2 contain highly acidic domains, whilst the C-terminal region unique for B23.1 is essential for its RNA-binding activity. Recently, we have shown that B23 interacts with adenoviral core proteins V, VII and pre-VII, and may have a role as a chaperone in the assembly of core proteins into the viral core (Samad *et al.*, 2007). However, an *in vivo* role(s) of B23 in the adenovirus life cycle has not yet been clarified. Here, we developed a decoy molecule for the interaction between B23 and core protein V based on analysis of their interaction domains. Furthermore, we studied the effect of small interfering RNA (siRNA)-mediated knockdown of B23 on adenovirus proliferation. Perturbation of B23 function by overexpression of the decoy molecule or by knockdown was shown to impede adenovirus proliferation without significant inhibition of viral DNA replication or viral late gene expression. However, chromatin immunoprecipitation (ChIP) experiments indicated that the association of core proteins and cellular histones with viral DNA was significantly increased following B23 knockdown. Taken together, these results suggest that B23 is required for maintenance of the proper adenovirus chromatin structure.

RESULTS

Domains of core protein V required for its interaction with B23

Recently, we showed that B23 interacts with adenoviral core proteins V and VII (Samad *et al.*, 2007). However, the function of B23 in adenovirus proliferation has not yet been clarified. To gain additional insight into the *in vivo* function of B23, we designed a decoy molecule based on analysis of the interaction domains between B23 and core protein V. First, we determined the domain of core protein V required for its interaction with B23. Core protein V contains lysine- and arginine-rich basic clusters in its N- and C-terminal regions. We postulated that core protein V would interacts with B23 through these basic clusters, as it has been shown that the acidic region of B23 is essential for its function (Okuwaki *et al.*, 2001a). To test this hypothesis, we constructed a series of deletion mutants, as shown in Fig. 1(a). GFP- and Flag-tagged core protein V mutants were co-expressed with haemagglutinin (HA)-tagged B23.1 in 293T cells, and immunoprecipitation assays were carried out with anti-Flag antibody. HA–B23.1 was co-immunoprecipitated with full-length core protein V (Fig. 1b, lane 10). The mutants V(1–313) and V(44–369), lacking the C- and N-terminal regions, respectively, bound similarly to HA–B23.1 (Fig. 1b, lanes 11 and 12). However, mutants V(44–313) and V(79–313), lacking both N- and C-terminal basic clusters showed virtually no ability to interact with HA–B23.1 (Fig. 1b, lanes 13 and 14). In contrast, the N- and C-terminal fragments, in the form of mutants V(1–78) and V(314–369), respectively, efficiently co-precipitated HA–B23.1 (Fig. 1b, lanes 15 and 16). These results indicated that both N- and C-terminal regions are involved in the interaction between B23 and core protein V, and that these fragments would be good candidates for decoy molecules for the interaction of core protein V with B23.

Inhibition of infectious virus production by B23 decoy molecule

We hypothesized that overexpression of these domains would interfere with the function of B23 in adenovirus proliferation if B23 is involved in the virus life cycle. To test this, HeLa cells were transfected with GFP-empty vector or with vectors for the expression of GFP–V, GFP–V(1–78), GFP–V(79–313) and GFP–V(314–369), and superinfected with human adenovirus type 5 (HAdV5) at 20 h post-transfection. At 24 h post-infection (p.i.), progeny virus particles were collected and the infectivity titre was determined as described in Methods [Figs 1c and S1 (available in JGV Online)]. The results demonstrated that overexpression of GFP–V, GFP–V(1–78) and GFP–V(314–369), but not of GFP alone or GFP–V(79–313), inhibited the production of infectious virus particles. These results suggested that the mutant proteins that tightly associated with B23 inhibited the infectious virus production. It was

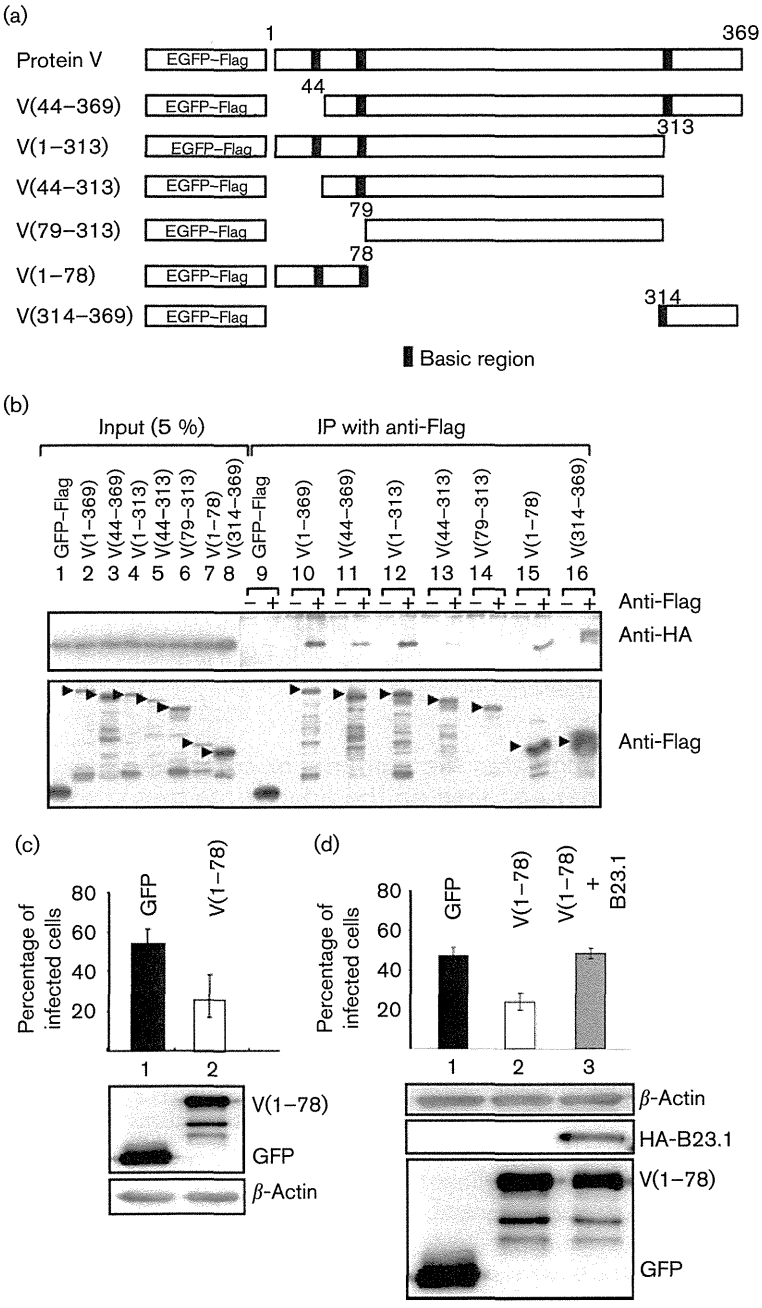

Fig. 1. N- and C-terminal regions of core protein V are required for the interaction with B23. (a) Schematic diagram of wild-type and mutant protein V constructs. GFP–Flag tag was fused at the N terminus of core protein V and its mutant proteins. The basic clusters of core protein V are indicated by filled boxes. (b) Immunoprecipitation of Flag-tagged core protein V. 293T cells were transiently co-transfected with HA–B23.1 and either GFP–Flag–protein V or its mutants. After immunoprecipitation without (–) or with (+) anti-Flag antibody, proteins in input extracts (lanes 1–8) and precipitated proteins (lanes 9–16) were separated by SDS-PAGE (12.5 % acrylamide) and detected by Western blotting with anti-HA and anti-Flag antibodies (top and bottom panels, respectively). The positions of GFP–Flag-tagged protein V and its mutants are indicated by arrowheads on the left of each lane. (c) Inhibition of virion production by a decoy molecule. HeLa cells were transfected with GFP-empty vector or a vector expressing GFP–Flag-tagged V(1–78) mutant. At 20 h post-transfection, cells were infected with HAdV5. At 24 h p.i., virus in the culture fluid was collected and virus titre was determined. In the lower panel, expression of exogenous proteins as well as β-actin was confirmed by Western blotting. (d) Rescue experiments. Cells were transfected with GFP–Flag (lane 1), GFP–Flag–V(1–78) with pCHA empty vector (lane 2) or GFP–Flag–V(1–78) with pCHA-B23.1 vector (lane 3). At 24 h post-transfection, the cells were superinfected with HAdV5 and virus production was examined as described in (c). Exogenously expressed proteins were detected by Western blotting, shown in the lower panel.

further demonstrated that co-expression of exogenous B23 with GFP–V(1–78) (Fig. 1d) rescued the negative effect of GFP–V(1–78). These results supported the idea that V(1–78) functions as a type of decoy for the interaction between B23 and core protein V, and that impairment of this interaction decreases the progeny virus production level.

B23 knockdown inhibits the production of infectious viral particles

To further demonstrate that B23 is involved in adenovirus proliferation, we decreased the cellular B23 level using siRNA specific for B23.1. Although both B23.1 and B23.2 have been suggested to be differentially involved in adenovirus replication (Hindley *et al.*, 2007), we focused on B23.1, as it is concentrated in the nucleolus, where core protein V is located at the late stage of infection (Matthews, 2001), whilst B23.2 is distributed throughout the nucleus. In addition, depletion of B23.1 alone was shown to efficiently decrease the nucleolar function of B23 (Murano *et al.*, 2008). Treatment of HeLa cells with B23.1 siRNA decreased the cellular B23.1 protein level but not that of β-actin, whereas control siRNA had no effect (Fig. 2a). The expression levels of another host factor for adenovirus remodelling, TAF-I, and other nucleolar proteins such as

nucleolin and fibrillarin were found to be unchanged following B23 knockdown (Fig. 2b). To examine the effect of B23 knockdown on adenovirus proliferation, control and B23.1 siRNA-treated HeLa cells were infected with HAdV5. We first examined the effect of siRNA treatment on the localization of viral proteins (Fig. 2c). In control siRNA-treated cells, DNA-binding protein (DBP) was concentrated in nuclear foci, whilst core protein VII was distributed throughout the nuclei at 24 h p.i. As reported previously (Hindley *et al.*, 2007; Matthews, 2001), the nucleolar localization of B23 was slightly suppressed following adenovirus infection, and B23 was partially co-localized with core protein VII but not with DBP. We also demonstrated that the localization patterns of DBP and core protein VII were not significantly affected by B23.1 siRNA treatment. At 24 h p.i., the supernatant fraction containing progeny virus particles was collected, cleared by low-speed centrifugation and examined to determine the infectious titre (Fig. 2d). The production of infectious progeny virus particles from B23 knockdown cells was decreased to approximately 50–60 % of that from control siRNA-treated cells (Fig. 2d, lanes 1 and 2). Even with the decreased B23.1 level, adenovirus production increased until 48 h p.i., although the amount of infectious virus produced from 24 to 36 h p.i. was lower than that in the control siRNA-treated cells (Figs 2c and S2). These results suggested that B23.1 is not essential but plays a crucial role in adenovirus production, and/or that other cellular factor(s) could also be involved (see Discussion). Next, we investigated whether the effect of B23 knockdown on adenovirus production could be rescued by B23 over-expression. At 36 h after the introduction of control or B23 siRNA, cells were transfected with empty vector or with vector encoding HA–B23.1. Cells were then infected with HAdV5 at 24 h after transfection of plasmid DNA and the production of progeny virus particles was examined. The expression levels of exogenous HA–B23.1 are shown in Fig. 2(e). Overexpression of B23.1 in control cells slightly inhibited infectious progeny virus production (Fig. 2d), although this result was not statistically significant. Importantly, exogenous expression of B23.1 counteracted the negative effect of B23.1 siRNA-mediated knockdown on progeny virus production. These results support the idea that B23.1 plays an important role in the production of infectious virus particles.

B23 knockdown has no significant effect on viral DNA replication and late gene expression

Given that B23 knockdown decreased the production of infectious virus particles, it was expected that this inhibition might be due to interference with viral DNA replication. To test this notion, control or B23 siRNA-treated HeLa cells were infected with HAdV5 and the amplification of viral DNA at 12, 18 and 24 h p.i. was examined by quantitative PCR (qPCR) using a primer set specific for adenoviral DNA (Fig. 3a). Because the amount of viral DNA increased as a function of incubation period after infection and the amplification of DNA was strongly inhibited by hydroxyurea, an inhibitor of DNA synthesis, it was confirmed that the PCR products detected under the conditions employed here corresponded to the amount of viral DNA. Surprisingly, no significant decrease in the amount of viral DNA was observed following B23 knockdown (Fig. 3a). We also examined the effect of B23 knockdown on viral late gene expression. The expression level of late genes was examined by Western blotting with anti-pVII and anti-V antibodies (Fig. 3b) and by RT-PCR with primer sets for mRNAs of the major late promoter (MLP) and pVII (Fig. 3c, d). Consistent with the fact that late gene transcription depends on viral DNA replication, the expression level of late genes was strongly inhibited by the presence of hydroxyurea. We did not find any significant decrease in mRNA and core protein expression levels following B23 knockdown (Fig. 3b–d). These results indicated that B23 plays a crucial role(s) in progeny virus production at a step(s) later than virus genome DNA replication and mRNA synthesis. As adenovirus genome replication depends completely on viral early gene products, we could exclude the possibility that B23 is involved in early gene transcription.

B23 regulates the amounts of core proteins and cellular histones on the adenovirus genome

Our biochemical data suggested that the adenoviral core proteins form aggregates with viral DNA when mixed directly, and that B23 dissociates the aggregation between the DNA and core proteins (Samad *et al.*, 2007). In addition, we demonstrated that B23, as a histone chaperone, regulates the histone density around the rRNA gene region in uninfected cells (Hisaoka *et al.*, 2010). Therefore, it is possible that B23 knockdown affects the virus genome chromatin structure in infected cells. To test this possibility, we examined whether B23 was associated with the virus genome in infected cells. HeLa cells were infected with HAdV5, and at 20 h p.i. cells were cross-linked with formaldehyde and then sonicated to release chromatin. The mean size of DNA purified from chromatin fragments was <1 kb (data not shown). The extracts were subjected to immunoprecipitation with antibodies against core proteins V and VII or B23. We found that B23 associated with the virus genome (the VA gene region), as did the core proteins V and VII (Fig. 4a). We examined the association of B23 with the virus genome using primer sets, as shown in Fig. 4(b, lower panel). Next, we assessed the amounts of core proteins and cellular histones on the virus genome with ChIP assays using cells treated with control and B23 siRNAs. HeLa cells treated with siRNAs were infected with HAdV5 at an m.o.i. of 10. At 20 h p.i., cells were subjected to ChIP assays, as described above. Five different primer sets, as shown in Fig. 4(b), were used to examine the amounts of core proteins and histones on the virus genome. In B23 knockdown cells, association of the core proteins V and VII with viral DNA was found to be increased in all regions tested (Fig. 4c, d). We also found that the association of histone H3 along the virus genome was increased (Fig. 4e).

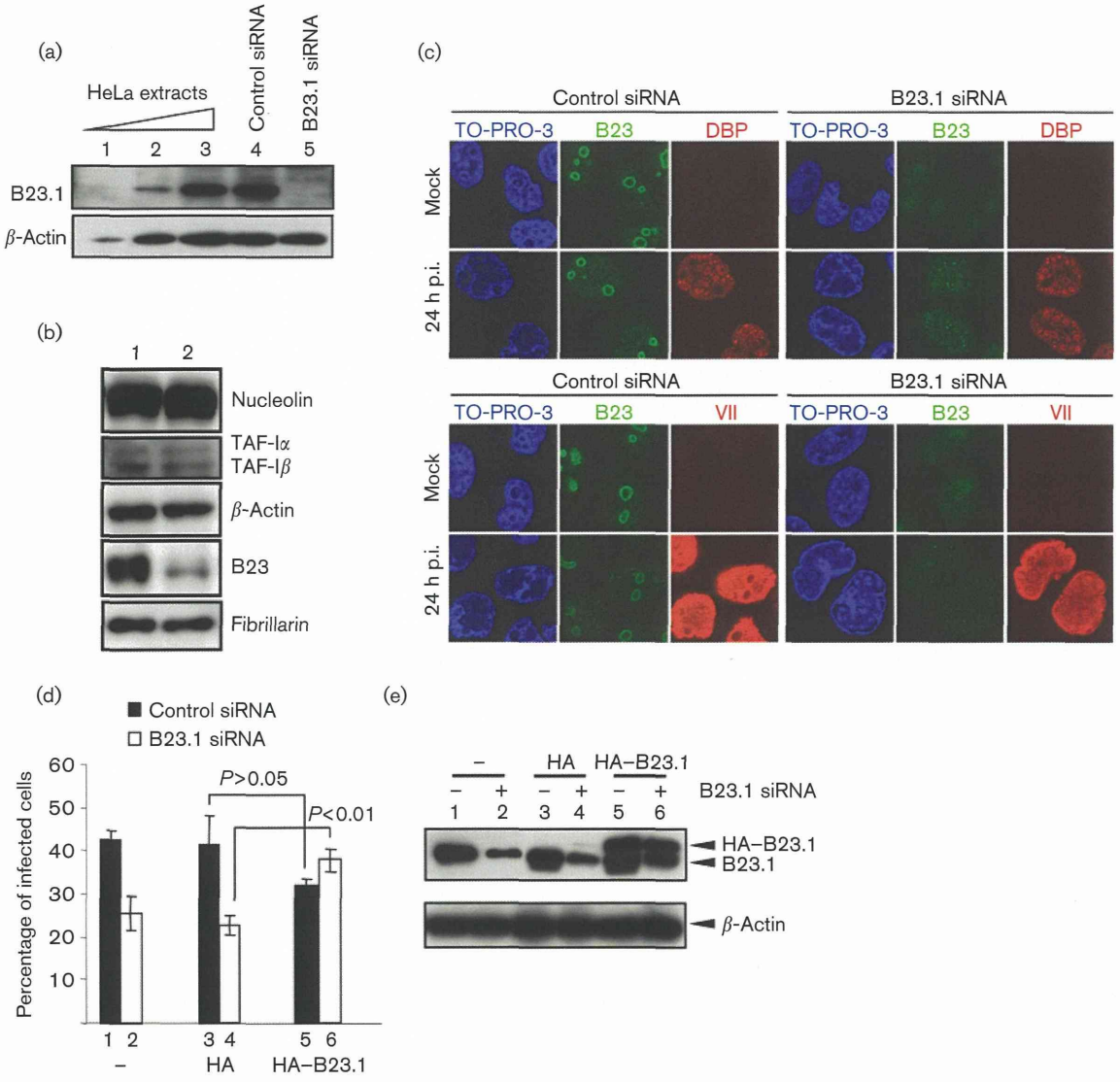

Fig. 2. B23 is involved in adenovirus proliferation. (a) Knockdown of B23.1. HeLa cells were transfected with control siRNA (lane 4) or B23 siRNA (lane 5), and the expression level of B23 was examined by Western blotting with anti-B23 antibody. HeLa cell lysates from 5×10^3, 1.5×10^4 and 5×10^4 cells (lanes 1–3, respectively) were loaded onto the same gel and used as standards. β-Actin is shown as a loading control. (b) Expression of nucleolar proteins. The expression levels of the indicated proteins were determined by Western blotting using HeLa cells treated with control siRNA (lane 1) or B23.1 siRNA (lane 2) as in (a). (c) Localization of viral proteins in B23.1 siRNA-treated cells. HeLa cells treated with control or B23.1 siRNA, as indicated, were superinfected with HAdV5 and subjected to indirect immunofluorescence analyses at 24 h p.i. B23 and DBP (top panels) or B23 and core protein VII (bottom panels) were simultaneously stained and visualized. Nuclei were counterstained with TO-PRO-3. (d) Inhibition of infectious virus production by knockdown of B23. HeLa cells treated with control or B23.1 siRNA were infected with HAdV5. At 24 h p.i., virus titres in the culture medium were determined as described in Methods (lanes 1 and 2). At 36 h after siRNA transfection, pCHA empty vector (lanes 3 and 4) or pCHA-B23.1 (lanes 5 and 6) was transfected into the cells and incubated for 24 h. The cells were then superinfected with HAdV5 and virus infectivity was determined at 24 h p.i., as described above. Experiments were carried out in triplicate and results are shown as means ± SD. Statistical *P* values are indicated at the top of the graph. (e) Expression level of endogenous and exogenous B23. Lysates prepared as described in (d) were analysed by Western blotting with anti-B23.1 and anti β-actin antibodies (top and bottom panels, respectively).

We also examined whether the amounts of core proteins and histone H3 on the virus genome increased by B23.1 knockdown were counteracted by exogenously expressed B23.1. HeLa cells treated with control or B23.1 siRNA were transiently transfected with empty and HA–B23.1 expression vectors and then infected with HAdV5. At

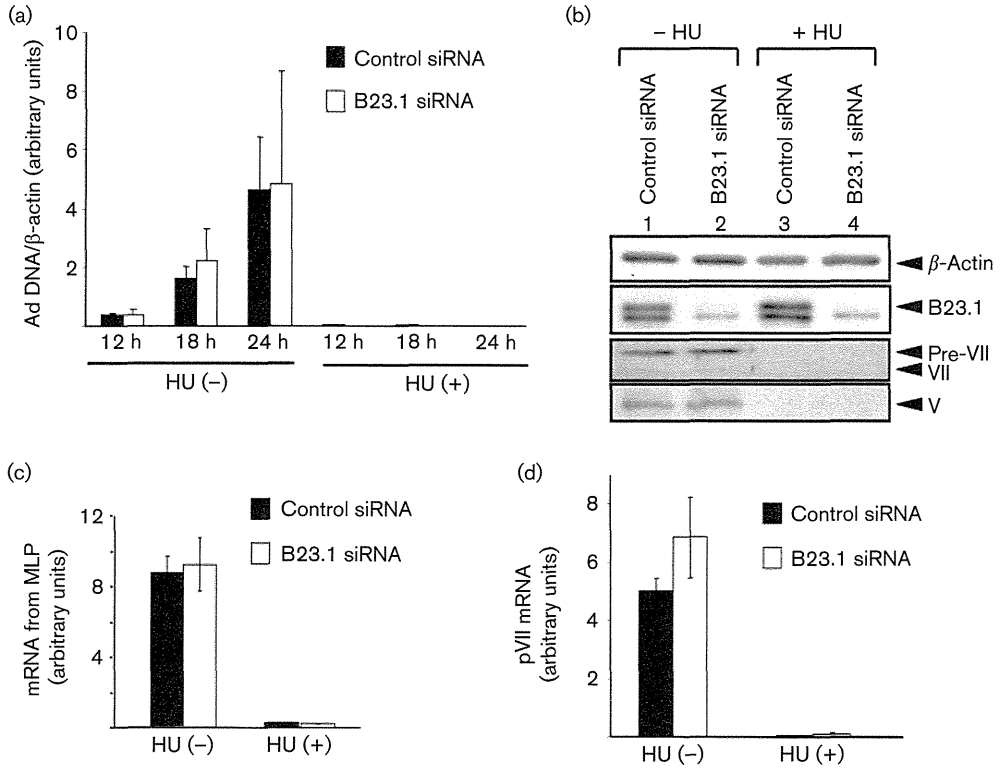

Fig. 3. Effect of B23 knockdown on adenoviral DNA replication and late gene expression. (a) Effect of B23.1 knockdown on adenoviral DNA replication. Control or B23.1 siRNA-treated HeLa cells were infected with HAdV5 and incubated without (−) or with (+) 2 mM hydroxyurea (HU). At 12, 18 and 24 h p.i., DNA was purified from the infected cells and the amount of viral DNA was examined by qPCR using a primer set specific for the VA region of the adenovirus genome. Genomic DNA purified from HeLa cells infected with HAdV5 was used as a standard for the amount of the virus genome in infected cells, and the relative amounts of adenoviral DNA were normalized to that of the β-actin gene. (b) Expression level of late gene products. Lysates were prepared from infected HeLa cells as described in (a) at 24 h p.i. Proteins were separated by SDS-PAGE, and analysed by Western blotting with antibodies against β-actin, B23 and core proteins V and pVII. (c, d) Expression levels of adenovirus late genes. HeLa cells treated with siRNA as described in (a) were infected with HAdV5. Total RNA was prepared at 18 h p.i., and the expression level of MLP mRNA (c) and pVII mRNA (d) was determined by qRT-PCR using specific primer sets, as described in Methods. PCRs were performed in triplicate and results are shown as means ± SD. Three independent experiments showed similar results.

24 h p.i., ChIP assays were carried out as shown in Fig. 4 using primer sets specific for the VA gene region (Fig. 5). Western blotting analyses demonstrated that the amount of B23.1 was decreased efficiently by siRNA treatment and was recovered by transient expression of exogenous HA–B23.1 (Fig. 5a, lanes 5 and 6). Consistent with the results in Fig. 4, the amounts of core proteins V and VII and histone H3 on the virus genome were increased by B23.1 knockdown (Fig. 5b–d). However, they were decreased following overexpression of HA–B23.1. Interestingly, even in control siRNA-treated cells, HA–B23.1 overexpression decreased the association levels of core protein V and histone H3. Taken together, these results suggest that B23 is involved in the regulation of viral chromatin formation in infected cells by restricting the access of core proteins and cellular histones.

DISCUSSION

In this paper, we studied the *in vivo* function of B23 in the adenovirus life cycle. Based on previous reports, it was expected that B23 might be involved in adenoviral DNA replication (Hindley *et al.*, 2007; Okuwaki *et al.*, 2001a). However, we could not detect any significant decrease in the amount of viral DNA (Fig. 3a) or the level of transcription or translation of core proteins (Fig. 3b–d) following B23.1 knockdown. Therefore, it is possible that B23.1 is not involved in adenoviral DNA replication in infected cells under the conditions used here or that loss of B23.1 may be compensated alternatively. In this sense, it should be noted that, as well as B23, other histone chaperones have also been identified as factors for adenoviral DNA replication (Kawase *et al.*,

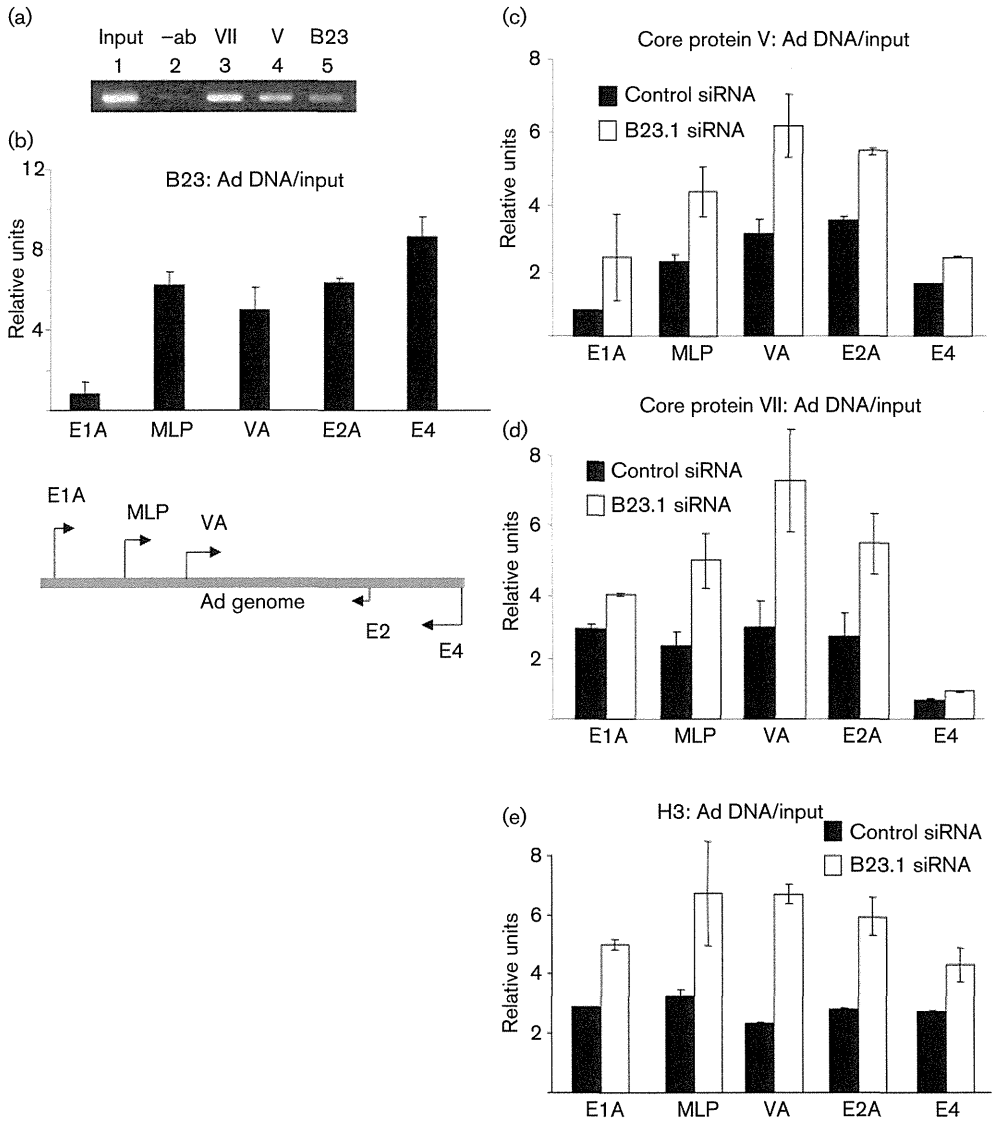

Fig. 4. Effect of B23 knockdown on adenovirus chromatin structure. (a) ChIP assays were carried out with extracts prepared from HAdV5-infected HeLa cells at 20 h p.i. DNA immunoprecipitated without (−ab, lane 2) or with anti-pVII, anti-V and anti-B23 antibodies (lanes 3–5, respectively) was examined by PCR using a primer set specific for the adenovirus VA gene. (b) B23 associates with the entire adenovirus genome in infected cells. DNA immunoprecipitated with anti-B23 as described in (a) was subjected to qPCR using primer sets specific for the adenovirus genome. The positions of the primer sets used are represented schematically in the lower panel. Arrows indicate the position and direction of transcription of each gene. DNA extracted from input extracts was used as a standard to quantify the amount of DNA immunoprecipitated with the anti-B23 antibody. (c–e) ChIP assay of adenovirus-infected HeLa cells treated with siRNAs. Control or B23.1 siRNA-treated HeLa cells were infected with HAdV5 and ChIP assays were carried out with antibodies against core proteins V (c) and pVII (d) and histone H3 (e). Immunoprecipitated DNA was examined by qPCR using the primer sets shown in (b). The amounts of immunoprecipitated DNA were analysed quantitatively and compared with those of DNAs extracted from input extracts. In (b–e), PCRs were carried out in triplicate and results are shown as means ± SD. Two independent experiments showed similar results.

1996; Matsumoto *et al.*, 1993; Okuwaki *et al.*, 2001a). In addition, we could not exclude the possibility that B23.2 that remains in B23.1 knockdown cells plays a compensatory role in adenoviral DNA replication. Nevertheless, the data presented here demonstrated that B23.1 knockdown did not significantly affect DNA replication and transcription.

We showed that the decrease in B23 reduced the production of progeny virions and increased the association level

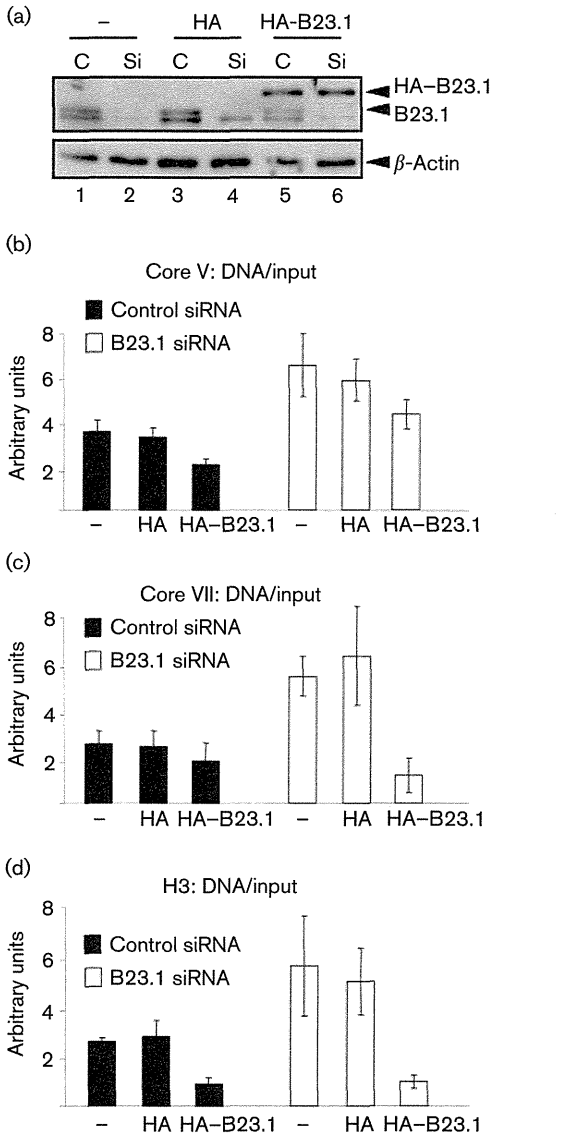

Fig. 5. Overexpression of exogenous B23.1 counteracts the effect of B23.1 knockdown on viral chromatin structure. (a) Expression levels of endogenous and exogenous B23.1. HeLa cells were treated with control (C) or B23.1 (Si) siRNA without (lanes 1 and 2) or with transfection of pCHA (lanes 3 and 4) or pCHA-B23.1 (lanes 5 and 6) and then infected with HAdV5. The expression levels of B23 and β-actin were examined by Western blotting. (b–d) ChIP assays. HeLa cells prepared as described in (a) were subjected to ChIP assays with antibodies against core proteins V (b) or VII (c) or histone H3 (d). Immunoprecipitated DNA was examined quantitatively by qPCR using primer sets specific for the adenovirus VA gene region. The amount of immunoprecipitated DNA was analysed quantitatively and compared with the DNA extracted from input extracts. PCRs were carried out in triplicate and results are shown asmeans ± SD.

of viral core proteins and cellular histones on the progeny virus genome DNA. Based on these observations, we propose that: (i) B23 is involved in the adenovirus infection cycle at a step after late gene expression, and (ii) proper virus chromatin assembly is required for adenovirus virion maturation. The precise mechanism of how B23 regulates viral chromatin and is involved in the final maturation step of infectious virus particles remains unclear. It is also possible that, in addition to B23, another cellular factor(s) is involved in these processes. TAF-I is a candidate for such an additional factor, as we have reported that TAF-I is also associated with pre-VII in the late phases of infection (Gyurcsik *et al.*, 2006). It is thought that the viral DNA associated with appropriate amounts of basic proteins is important for encapsidation. In fact, the adenovirus genome DNA is condensed into a core structure only by viral basic proteins within virions, although viral DNA is associated with histones throughout the infection cycle (Déry *et al.*, 1985; Levy & Noll, 1981). Thus, it is likely that those virus genomes associated with cellular histones are restricted and eliminated for encapsidation. For efficient encapsidation to occur, cellular histones must be replaced with viral basic proteins through an unknown pathway.

Newly replicated DNA is associated with histones, and this viral DNA–histone complex may be important for ongoing replication and transcription throughout the infection cycle. At later stages of infection, the synthesis of cellular DNA and histones is inhibited, with the concomitant accumulation of a large pool of viral basic proteins. The virus genomic DNA associated with viral core proteins might become prominent through direct interaction of ongoing replicated DNA with viral basic proteins and/or replacement of histones on the replicated DNA with viral basic proteins. Based on these observations, B23 may be involved in the final encapsidation step, either by replacing histones with core proteins or by restricting the access of excessive amounts of viral basic proteins/histones to viral DNA. These models are in agreement with earlier assumptions (Déry *et al.*, 1985; Komatsu *et al.*, 2011).

METHODS

Cell culture and viruses. HeLa cells were maintained in minimal essential medium (MEM; Nissui) supplemented with 10 % FBS at 37 °C. 293T cells were cultured at 37 °C in Dulbecco's modified Eagle's medium (Nissui) containing 10 % FBS. The HAdV5 used in this study was amplified and purified as described previously (Haruki *et al.*, 2006).

Plasmid construction and transfection. The construction of plasmids for a series of protein V mutants is described in the Supplementary Methods. pCHA-B23.1 was prepared as described by Okuwaki *et al.* (2002). Transient transfection of each plasmid was performed by the calcium phosphate precipitation method into 293T cells and by Gene-Juice (Novagen) into HeLa cells.

Antibodies. The antibodies used in this study were as follows. Mouse mAb for B23 that recognizes endogenous B23.1 was purchased from Invitrogen. Polyclonal antibody recognizing both B23.1 and B23.2 was generated in rabbits using B23ΔC2 expressed in *Escherichia coli* (Okuwaki *et al.*, 2001a) as an antigen. Rabbit anti-core protein V and

mouse anti-DBP antibodies were obtained from Professor W. C. Russell (University of St Andrews, Fife, UK) as a generous donation. The rat polyclonal anti-pre-VII (Haruki *et al.*, 2003), mouse mAb against Flag tag, rabbit mAb against HA, rabbit polyclonal antibody against histone H3 and mouse mAb against β-actin have been described elsewhere (Murano *et al.*, 2008).

Immunoprecipitation assays. 293T cells, transiently transfected with plasmids where indicated, were lysed in 1 ml immunoprecipitation buffer [50 mM Tris/HCl (pH 7.9), 1 mM PMSF, 0.1 % Triton X-100, 1 mg BSA ml^{-1}] containing 150 mM NaCl on ice for 10 min followed by extensive sonication. Cell extracts recovered by centrifugation were mixed with anti-Flag antibody and incubated at 4 °C for 3 h. Protein A–Sepharose beads (10 μl resin; GE Healthcare) were added and the mixture was further incubated for 1 h with gentle agitation. The beads were washed three times with 0.5 ml immunoprecipitation buffer. Immunoprecipitated proteins were eluted by the addition of SDS sample buffer, and boiled, separated by SDS-PAGE (12.5 % acrylamide) and transferred to PVDF membrane (Millipore). The membrane was subjected to Western blotting analysis using anti-HA antibody.

Decoy assays. HeLa cells were transfected with GFP-empty vector or with vector for the expression of GFP–V(1–78). At 20 h post-transfection, cells were superinfected with HAdV5 at an m.o.i. of 10. At 24 h p.i., culture supernatant (5 μl), clarified by low-speed centrifugation, was used for infection of HeLa cells seeded on coverslips in 12-well plates (1×10^5 cells per well) to determine the virus titre. After incubation for 1 h, cells were supplemented with MEM containing 2 % FBS and maintained at 37 °C in a 5 % CO_2 environment for an additional 15 h. The cells on coverslips were collected, washed with PBS, fixed with 3 % paraformaldehyde for 10 min at room temperature and stained with anti-DBP antibody. Cells were counterstained with DAPI to stain the nuclei, and infectious titres (percentage of infected cells) were determined by counting DBP-positive cells compared with DAPI-positive cells. The assay was carried out in duplicate and the results are given as means ± SD.

B23 knock down by siRNA. Stealth RNAi negative control and B23 Stealth RNAi (NPM1-HSS143154; Invitrogen) were introduced into HeLa cells using Lipofectamine RNAiMAX (Invitrogen) according to the manufacturer's protocol. At 24 h post-transfection, the medium was replaced and the cells were harvested at 60 h after siRNA transfection. Total HeLa cell lysates were prepared, and proteins were separated by SDS-PAGE (10 % acrylamide) and detected by Western blotting. To examine the effect of B23 knockdown on virus production, control and B23 siRNA-treated HeLa cells at 60 h post-transfection were infected with HAdV5 at an m.o.i. of 10. After 24 h, the culture medium was recovered and the virus titre determined, as described above.

Immunofluorescence assays. Indirect immunofluorescence assays were carried out essentially as described previously (Haruki *et al.*, 2006). Briefly, cells grown on 15 mm coverslips (Matsunami) were fixed with 4 % paraformaldehyde in PBS for 10 min at room temperature and then treated with 0.5 % NP-40 in PBS for 5 min at room temperature. After blocking with 5 % non-fat milk in TBS with 0.1 % Tween 20, samples were subjected to immunofluorescence analyses using the antibodies described above. Proteins were visualized with secondary antibodies (AlexaFluor 488-conjugated anti-rabbit IgG, AlexaFluor 568-conjugated anti-mouse IgG and AlexaFluor 568-conjugated anti-rat IgG; Invitrogen). DNA was visualized by staining with TO-PRO-3 iodide (Invitrogen). Labelled cells were observed by confocal laser-scanning microscopy (LSM5 Exciter; Carl Zeiss) using argon laser (488 nm) and He/Ne laser (546 and 633 mm) lines.

qPCR. Control and B23 siRNA-treated HeLa cells were infected with HAdV5 at an m.o.i. of 10. At 12, 18 and 24 h p.i., cells (1×10^5) were collected and suspended in lysis buffer [20 mM Tris/HCl (pH 7.9), 100 mM NaCl, 5 mM EDTA, 0.5 % SDS] and total DNA was purified by proteinase K treatment overnight at 50 °C, followed by phenol/chloroform extraction and ethanol precipitation. The amount of DNA was then examined by qPCR with a primer set specific for the adenovirus VA gene region (see below). Total RNA was purified from infected cells (1×10^5) using an RNeasy Mini kit (Qiagen), and the purified RNA was treated with DNase I according to the manufacturer's protocol. The concentration of RNA in each sample was determined using NanoDrop (Thermo Scientific). cDNA was synthesized from total RNA (1 μg) using ReverTraAce (Toyobo) and oligo-dT as primer according to the manufacturer's protocol. qPCR with FastStart SYBER Green Master Mix (Roche) and a Thermal Cycler Dice Real-time System (Takara) was performed using synthesized cDNA as template with primer sets specific for the mRNA from the MLP (5′-ACTCTCTTCCGCATCGCTGT-3′ and 5′-GTGACTG-GTTAGACGCCTTTCT-3′) and β-actin (5′-ATGGGTCAGAAGG-ATTCCTATGT-3′ and 5′-GGTCATCTTCTCGCGGTT-3′) genes.

ChIP assays. ChIP assays were carried out as described by the manufacturer (ChIP Assay kit; Millipore) with antibodies against core proteins V and pVII, B23 and histone H3. The amount of immunoprecipitated DNA was determined by qPCR as described above. The reaction conditions have been described previously (Komatsu *et al.*, 2011). The following primer sets were used: 5′-GGGTCAAAGT-TGGCGTTTTA-3′ and 5′-CAAAATGGCTAGGAGGTGGA-3′ for the E1a promoter region, 5′-GCGGTCCTCCTCGTATAGAA-3′ and 5′-CCCACCCCCTTTTATAGCC-3′ for the MLP region, 5′-GCTG-GAGCAAAACCCAAATA-3′ and 5′-TATCTTGCGGG-CGTAAAACT-3′ for the VA region, 5′-GTGTAGACACTTAAGCTCGCCTT-3′ and CTTCAAACTGCCTGACCAAGT-3′ for the E2A (DBP) region, and 5′-TGGCGTGGTCAAACTCTACA-3′ and 5′-GATTTTTACAATGGCCG-GACT-3′ for the E4 ORF region.

ACKNOWLEDGEMENTS

We thank Professor W. C. Russell for providing anti-V and anti-DBP antibodies. This work was supported in part by grants-in-aid from the Ministry of Culture, Sports, Science, and Technology of Japan (to K. N. and M. O.), Special Coordination Funds for Promoting Science and Technology (to M. O.), and a research fellowship of the Japan Society for the Promotion of Science (JSPS) (to M. A. S.).

REFERENCES

Adachi, Y., Copeland, T. D., Hatanaka, M. & Oroszlan, S. (1993). Nucleolar targeting signal of Rex protein of human T-cell leukemia virus type I specifically binds to nucleolar shuttle protein B-23. *J Biol Chem* **268**, 13930–13934.

Anderson, C. W., Young, M. E. & Flint, S. J. (1989). Characterization of the adenovirus 2 virion protein, mu. *Virology* **172**, 506–512.

Black, B. C. & Center, M. S. (1979). DNA-binding properties of the major core protein of adenovirus 2. *Nucleic Acids Res* **6**, 2339–2353.

Brown, D. T., Westphal, M., Burlingham, B. T., Winterhoff, U. & Doerfler, W. (1975). Structure and composition of the adenovirus type 2 core. *J Virol* **16**, 366–387.

Chatterjee, P. K., Vayda, M. E. & Flint, S. J. (1985). Interactions among the three adenovirus core proteins. *J Virol* **55**, 379–386.

Chatterjee, P. K., Vayda, M. E. & Flint, S. J. (1986). Adenoviral protein VII packages intracellular viral DNA throughout the early phase of infection. *EMBO J* **5**, 1633–1644.

Chen, J., Morral, N. & Engel, D. A. (2007). Transcription releases protein VII from adenovirus chromatin. *Virology* **369**, 411–422.

Daniell, E., Groff, D. E. & Fedor, M. J. (1981). Adenovirus chromatin structure at different stages of infection. *Mol Cell Biol* **1**, 1094–1105.

Déry, C. V., Toth, M., Brown, M., Horvath, J., Allaire, S. & Weber, J. M. (1985). The structure of adenovirus chromatin in infected cells. *J Gen Virol* **66**, 2671–2684.

Fedor, M. J. & Daniell, E. (1983). Ionic and nonionic interactions in adenoviral nucleoprotein complexes. *J Virol* **47**, 370–375.

Greber, U. F., Webster, P., Weber, J. & Helenius, A. (1996). The role of the adenovirus protease on virus entry into cells. *EMBO J* **15**, 1766–1777.

Gyurcsik, B., Haruki, H., Takahashi, T., Mihara, H. & Nagata, K. (2006). Binding modes of the precursor of adenovirus major core protein VII to DNA and template activating factor I: implication for the mechanism of remodeling of the adenovirus chromatin. *Biochemistry* **45**, 303–313.

Haruki, H., Gyurcsik, B., Okuwaki, M. & Nagata, K. (2003). Ternary complex formation between DNA–adenovirus core protein VII and TAF-Iβ/SET, an acidic molecular chaperone. *FEBS Lett* **555**, 521–527.

Haruki, H., Okuwaki, M., Miyagishi, M., Taira, K. & Nagata, K. (2006). Involvement of template-activating factor I/SET in transcription of adenovirus early genes as a positive-acting factor. *J Virol* **80**, 794–801.

Hindley, C. E., Davidson, A. D. & Matthews, D. A. (2007). Relationship between adenovirus DNA replication proteins and nucleolar proteins B23.1 and B23.2. *J Gen Virol* **88**, 3244–3248.

Hingorani, K., Szebeni, A. & Olson, M. O. (2000). Mapping the functional domains of nucleolar protein B23. *J Biol Chem* **275**, 24451–24457.

Hisaoka, M., Ueshima, S., Murano, K., Nagata, K. & Okuwaki, M. (2010). Regulation of nucleolar chromatin by B23/nucleophosmin jointly depends upon its RNA binding activity and transcription factor UBF. *Mol Cell Biol* **30**, 4952–4964.

Johnson, J. S., Osheim, Y. N., Xue, Y., Emanuel, M. R., Lewis, P. W., Bankovich, A., Beyer, A. L. & Engel, D. A. (2004). Adenovirus protein VII condenses DNA, represses transcription, and associates with transcriptional activator E1A. *J Virol* **78**, 6459–6468.

Kawase, H., Okuwaki, M., Miyaji, M., Ohba, R., Handa, H., Ishimi, Y., Fujii-Nakata, T., Kikuchi, A. & Nagata, K. (1996). NAP-I is a functional homologue of TAF-I that is required for replication and transcription of the adenovirus genome in a chromatin-like structure. *Genes Cells* **1**, 1045–1056.

Komatsu, T., Haruki, H. & Nagata, K. (2011). Cellular and viral chromatin proteins are positive factors in the regulation of adenovirus gene expression. *Nucleic Acids Res* **39**, 889–901.

Levy, A. & Noll, M. (1981). Chromatin fine structure of active and repressed genes. *Nature* **289**, 198–203.

Martin-Fernandez, M., Longshaw, S. V., Kirby, I., Santis, G., Tobin, M. J., Clarke, D. T. & Jones, G. R. (2004). Adenovirus type-5 entry and disassembly followed in living cells by FRET, fluorescence anisotropy, and FLIM. *Biophys J* **87**, 1316–1327.

Matsumoto, K., Nagata, K., Ui, M. & Hanaoka, F. (1993). Template activating factor I, a novel host factor required to stimulate the adenovirus core DNA replication. *J Biol Chem* **268**, 10582–10587.

Matsumoto, K., Okuwaki, M., Kawase, H., Handa, H., Hanaoka, F. & Nagata, K. (1995). Stimulation of DNA transcription by the replication factor from the adenovirus genome in a chromatin-like structure. *J Biol Chem* **270**, 9645–9650.

Matthews, D. A. (2001). Adenovirus protein V induces redistribution of nucleolin and B23 from nucleolus to cytoplasm. *J Virol* **75**, 1031–1038.

Murano, K., Okuwaki, M., Hisaoka, M. & Nagata, K. (2008). Transcription regulation of the rRNA gene by a multifunctional nucleolar protein, B23/nucleophosmin, through its histone chaperone activity. *Mol Cell Biol* **28**, 3114–3126.

Nagata, K., Kawase, H., Handa, H., Yano, K., Yamasaki, M., Ishimi, Y., Okuda, A., Kikuchi, A. & Matsumoto, K. (1995). Replication factor encoded by a putative oncogene, *set*, associated with myeloid leukemogenesis. *Proc Natl Acad Sci U S A* **92**, 4279–4283.

Nakanishi, Y., Maeda, K., Ohtsuki, M., Hosokawa, K. & Natori, S. (1986). *In vitro* transcription of a chromatin-like complex of major core protein VII and DNA of adenovirus serotype 2. *Biochem Biophys Res Commun* **136**, 86–93.

Nakano, M. Y., Boucke, K., Suomalainen, M., Stidwill, R. P. & Greber, U. F. (2000). The first step of adenovirus type 2 disassembly occurs at the cell surface, independently of endocytosis and escape to the cytosol. *J Virol* **74**, 7085–7095.

Okuda, M., Horn, H. F., Tarapore, P., Tokuyama, Y., Smulian, A. G., Chan, P.-K., Knudsen, E. S., Hofmann, I. A., Snyder, J. D. & other authors (2000). Nucleophosmin/B23 is a target of CDK2/cyclin E in centrosome duplication. *Cell* **103**, 127–140.

Okuwaki, M., Iwamatsu, A., Tsujimoto, M. & Nagata, K. (2001a). Identification of nucleophosmin/B23, an acidic nucleolar protein, as a stimulatory factor for *in vitro* replication of adenovirus DNA complexed with viral basic core proteins. *J Mol Biol* **311**, 41–55.

Okuwaki, M., Matsumoto, K., Tsujimoto, M. & Nagata, K. (2001b). Function of nucleophosmin/B23, a nucleolar acidic protein, as a histone chaperone. *FEBS Lett* **506**, 272–276.

Okuwaki, M., Tsujimoto, M. & Nagata, K. (2002). The RNA binding activity of a ribosome biogenesis factor, nucleophosmin/B23, is modulated by phosphorylation with a cell cycle-dependent kinase and by association with its subtype. *Mol Biol Cell* **13**, 2016–2030.

Okuwaki, M., Kato, K., Shimahara, H., Tate, S. & Nagata, K. (2005). Assembly and disassembly of nucleosome core particles containing histone variants by human nucleosome assembly protein I. *Mol Cell Biol* **25**, 10639–10651.

Samad, M. A., Okuwaki, M., Haruki, H. & Nagata, K. (2007). Physical and functional interaction between a nucleolar protein nucleophosmin/B23 and adenovirus basic core proteins. *FEBS Lett* **581**, 3283–3288.

Savkur, R. S. & Olson, M. O. (1998). Preferential cleavage in pre-ribosomal RNA by protein B23 endoribonuclease. *Nucleic Acids Res* **26**, 4508–4515.

Sergeant, A., Tigges, M. A. & Raskas, H. J. (1979). Nucleosome-like structural subunits of intranuclear parental adenovirus type 2 DNA. *J Virol* **29**, 888–898.

Spector, D. J. (2007). Default assembly of early adenovirus chromatin. *Virology* **359**, 116–125.

Sung, M. T., Lischwe, M. A., Richards, J. C. & Hosokawa, K. (1977). Adenovirus chromatin I. Isolation and characterization of the major core protein VII and precursor Pro-VII. *J Biol Chem* **252**, 4981–4987.

Sung, M. T., Cao, T. M., Coleman, R. T. & Budelier, K. A. (1983). Gene and protein sequences of adenovirus protein VII, a hybrid basic chromosomal protein. *Proc Natl Acad Sci U S A* **80**, 2902–2906.

Tate, V. E. & Philipson, L. (1979). Parental adenovirus DNA accumulates in nucleosome-like structures in infected cells. *Nucleic Acids Res* **6**, 2769–2785.

Trotman, L. C., Mosberger, N., Fornerod, M., Stidwill, R. P. & Greber, U. F. (2001). Import of adenovirus DNA involves the nuclear pore complex receptor CAN/Nup214 and histone H1. *Nat Cell Biol* **3**, 1092–1100.

Xue, Y., Johnson, J. S., Ornelles, D. A., Lieberman, J. & Engel, D. A. (2005). Adenovirus protein VII functions throughout early phase and interacts with cellular proteins SET and pp32. *J Virol* **79**, 2474–2483.

Yu, Y., Maggi, L. B., Jr, Brady, S. N., Apicelli, A. J., Dai, M. S., Lu, H. & Weber, J. D. (2006). Nucleophosmin is essential for ribosomal protein L5 nuclear export. *Mol Cell Biol* **26**, 3798–3809.

J Biol Inorg Chem (2013) 18:309–321
DOI 10.1007/s00775-013-0975-7

ORIGINAL PAPER

The role of the N-terminal loop in the function of the colicin E7 nuclease domain

Anikó Czene · Eszter Németh · István G. Zóka · Noémi I. Jakab-Simon · Tamás Körtvélyesi · Kyosuke Nagata · Hans E. M. Christensen · Béla Gyurcsik

Received: 18 September 2012 / Accepted: 31 December 2012 / Published online: 19 January 2013

Abstract Colicin E7 (ColE7) is a metallonuclease toxin of *Escherichia coli* belonging to the HNH superfamily of nucleases. It contains highly conserved amino acids in its $HHX_{14}NX_8HX_3H$ ββα-type metal ion binding C-terminal active centre. However, the proximity of the arginine at the N-terminus of the nuclease domain of ColE7 (NColE7, 446–576) is necessary for the hydrolytic activity. This poses a possibility of allosteric activation control in this protein. To obtain more information on this phenomenon, two protein mutants were expressed, i.e. four and 25 N-terminal amino acids were removed from NColE7. The effect of the N-terminal truncation on the Zn^{2+} ion and DNA binding as well as on the activity was investigated in this study by mass spectrometry, synchrotron-radiation circular dichroism and fluorescence spectroscopy and agarose gel mobility shift assays. The dynamics of protein backbone movement was simulated by molecular dynamics. Semiempirical quantum chemical calculations were performed to obtain better insight into the structure of the active centre. The longer protein interacted with both Zn^{2+} ion and DNA more strongly than its shorter counterpart. The results were explained by the structural stabilization effect of the N-terminal amino acids on the catalytic centre. In agreement with this, the absence of the N-terminal sequences resulted in significantly increased movement of the backbone atoms compared with that in the native NColE7: in ΔN25-NColE7 the amino acid strings between residues 485–487, 511–515 and 570–571, and in ΔN4-NColE7 those between residues 467–468, 530–535 and 570–571.

Keywords Metallonuclease · Colicin E7 · N-terminally truncated mutants · Zinc(II) binding

Introduction

Colicin E7 (ColE7) is a metallonuclease toxin of *Escherichia coli* [1]. Its role is to protect the host cell from other

Electronic supplementary material The online version of this article (doi:10.1007/s00775-013-0975-7) contains supplementary material, which is available to authorized users.

A. Czene · E. Németh · I. G. Zóka · N. I. Jakab-Simon · B. Gyurcsik (✉)
Department of Inorganic and Analytical Chemistry,
University of Szeged,
Dóm tér 7, Szeged 6720, Hungary
e-mail: gyurcsik@chem.u-szeged.hu

A. Czene · B. Gyurcsik
Bioinorganic Chemistry Research Group of Hungarian Academy of Sciences,
Dóm tér 7, Szeged 6720, Hungary

E. Németh · T. Körtvélyesi
Department of Physical Chemistry and Material Sciences,
University of Szeged,
Aradi Vértanuk tere 1, Szeged 6720, Hungary

N. I. Jakab-Simon · H. E. M. Christensen
Department of Chemistry,
Technical University of Denmark,
Kemitorvet, Building 207,
2800 Kongens Lyngby, Denmark

K. Nagata
Department of Infection Biology,
Graduate School of Comprehensive Human Sciences and Faculty of Medicine,
University of Tsukuba,
1-1-1 Tennodai, Tsukuba 305-8575, Japan

related bacteria and bacteriophages [2] by degradation of their chromosomal DNA during environmental stress. To exert cell-killing activity, ColE7 has to get across both the outer and the inner cell membrane, facilitated by the receptor-binding and translocation domains [3, 4]. The host cell itself is protected by the simultaneously expressed immunity protein Im7 blocking the DNA binding site [5, 6] of the nuclease domain of ColE7 (NColE7) owing to tight interactions based on charge complementarity [7–12].

ColE7 belongs to the HNH superfamily of nucleases [13–15] possessing a 30–40 amino acid long ββα-type metal ion binding motif in their active centre. The amino acids histidine and asparagine are highly conserved within the sequence $HHX_{14}NX_8HX_3H$ corresponding to this motif at the C-terminal region of bacterial colicins and pyocins [16, 17]. At the same time, the HNH motif is found in various regions of a wide range of enzymes, including group I homing endonucleases (e.g. I-Hmu-I [18]), procaryotic extracellular nucleases (nuclease A [19]) and also in an increasing number of restriction endonucleases (e.g. *Mnl*I [20], *Kpn*I [21, 22], *Hph*I [23], *Eco*31I [24], *Hpy*99I [25]). Sequences are collected in the HNH [26] and Pfam [27] databases. The first histidine (H) in the name-giving HNH amino acids acts as the general base in DNA hydrolysis. The asparagine (N) residue plays a structural role constraining the HNH loop by extensive hydrogen-bonding interactions [14, 28]. The third conserved residue in the HNH string is a metal-binding histidine. The HNH motif of ColE7 binds to the 3′ site of the scissile phosphate in the minor groove of the DNA, whereas the other parts of the nuclease domain provide strong, non-specific binding within the major groove [16, 29], similarly to colicin E9 (ColE9) [30, 31]. As such, NColE7 catalyses the non-specific hydrolysis of nucleic acids.

There is still debate about the role of the different divalent metal ions in colicin nucleases [30–38]. In NColE7, three histidine side chains bind a metal cofactor, which is most probably Zn^{2+} ion under physiological conditions [32], but the apoprotein can be reactivated to a different extent by other divalent metal ions such as Mn^{2+}, Ni^{2+}, Co^{2+}, Cu^{2+}, Mg^{2+}, Ca^{2+} and Sr^{2+} [5, 39]. The metal ion, having a free coordination site, has essential multiple roles in DNA cleavage: it binds to the scissile phosphodiester, polarizes the P–O bond for nucleophilic attack and stabilizes the phosphoanion transition state and the leaving group. As mentioned above, the attacking nucleophilic OH^- is supposed to be generated by the most conserved histidine residue of the HNH motif—which does coordinate to the Zn^{2+} ion. The hydrolytic reaction is also facilitated by the 19° bending of the DNA due to the protein binding [32]. The Zn^{2+} ion is not required for DNA binding, but it is essential for DNA hydrolysis [39].

In a recent article [40] it was demonstrated that during the membrane translocation process the periplasmic extracts cleave ColE7 between K446 and R447 and only the nuclease domain (R447–K576) enters the cell. The R447E ColE7 mutant lost its cell-killing activity owing to failed inner membrane translocation, but the K446E and N448A mutants retained it. However, it was shown in an in vitro assay that the R447E mutant of NColE7 (444–576) has only approximately 15 % of the endonuclease activity of the wild-type NColE7. This difference was assumed to be the consequence of lower affinity for DNA and not a consequence of the decrease in catalytic activity. On the basis of the crystal structure of Vvn endonuclease with DNA, it was proposed that the role of such a spatially close arginine residue might also be to stabilize the enzyme–product complex [41].

The necessity of the N-terminal amino acids in NColE7 for the function of the C-terminal catalytic centre poses the possibility of an allosteric activation within the enzyme that would be a desired property for use in an artificial nuclease [42]. The N-terminal end of NColE7 forms a loop leaning near to the active centre, and the interactions between them might be decisive in control of the function. In this work, two N-terminally truncated derivatives of NColE7 (446–576)—glutathione *S*-transferase (GST)–ΔN25-NColE7 and GST-ΔN4-NColE7-C* (instead of the GST-ΔN4-NColE7 protein we studied its C-terminal mutant GST-ΔN4-NColE7-C* selected by bacterial cells; the sequences are defined in Fig. 1a)—were expressed in *E. coli*. The proteins with and without the GST tag were purified for the studies of DNA- and Zn^{2+}-binding activities. Gel mobility shift assay, synchrotron-radiation circular dichroism (SRCD) spectroscopy, fluorescence spectroscopy and mass spectrometry experiments were performed and were complemented by bioinformatics, molecular dynamics and semiempirical quantum chemical calculations. The results will lead us to a better understanding of the role of the N-terminal loop in the catalysed reaction as well as its structural effects.

Materials and methods

Cloning, protein expression and purification

The genes of the mutant proteins were amplified by PCR from the pQE70 plasmid (a generous gift from K.-F. Chak, Institute of Biochemistry and Molecular Biology, National Yang Ming University, Taipei, Taiwan) by using the oligonucleotides ΔN4-NColE7-F: 5′-ggaattccagggaaggcaacaggta-3′ and ΔN25-NColE7-F: 5′-ggaattcgacttaggttctcctgttcca-3′ as forward primers and NColE7-R: 5′-gccgctcgagcta tttacctcggtgaatatcaatatgc-3′ as the reverse primer and

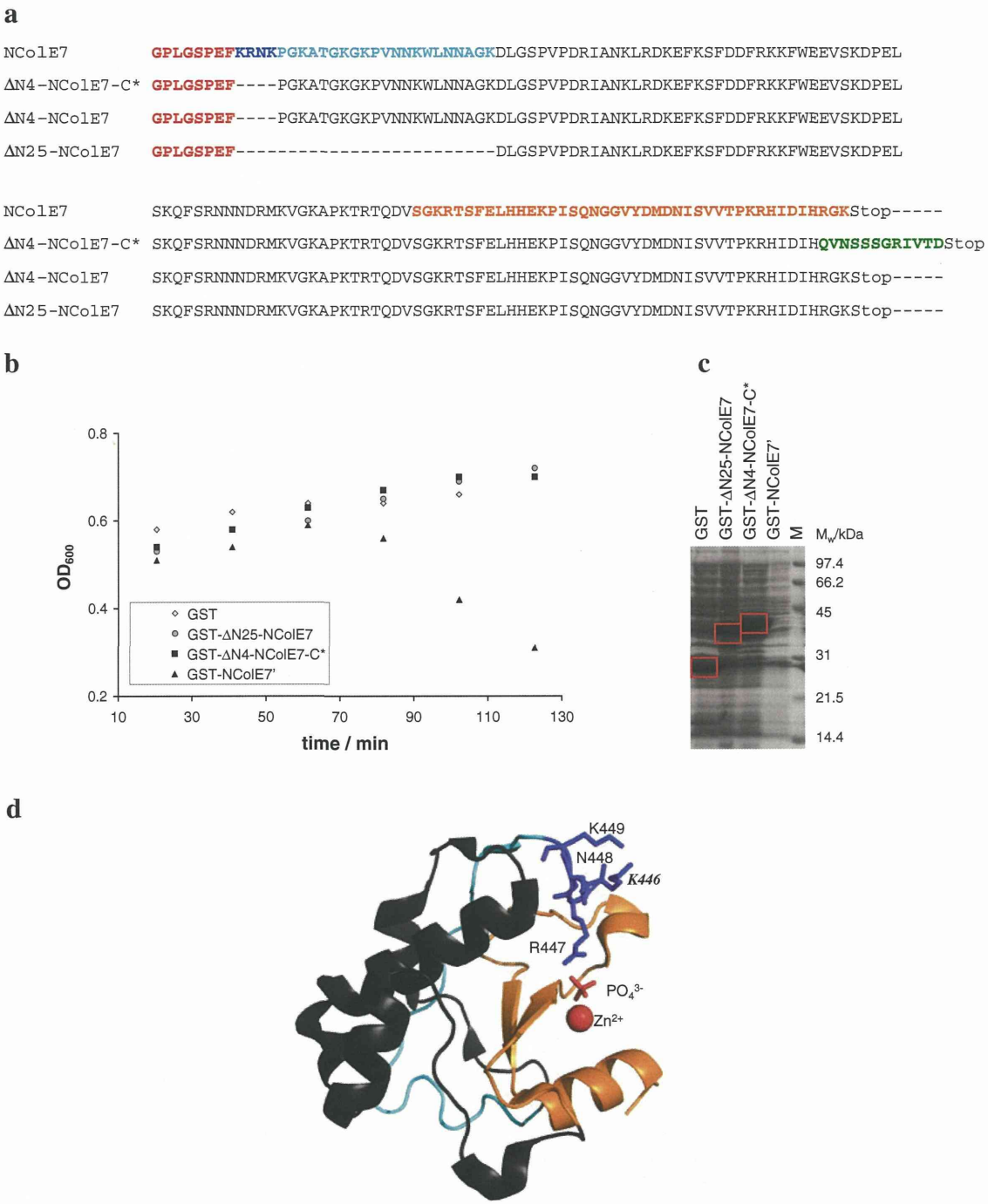

Fig. 1 **a** The sequences of the nuclease domain of colicin E7 (NColE7) [from K446 to K576 according to the original colicin E7 (ColE7) numbering] and the deletion mutants ΔN4-NColE7-C*, ΔN4-NColE7 and ΔN25-NColE7. The amino acids in *red* are fused to the N-terminus as a consequence of expression and purification from the pGEX-6-P1 vector and cleavage by PreScission protease. The amino acids in *green* indicate the result of the random mutation of the C-terminus in ΔN4-NColE7-C*. All the residues in *blue* are cut from ΔN25-NColE7 and only the residues in *dark blue* are from ΔN4-NColE7(-C*), and the HNH motif is in *orange*, similarly to **d**. **b** Growth of the *Escherichia coli* cells expressing different glutathione *S*-transferase (*GST*) protein variants after induction with isopropyl β-thiogalactoside as monitored by measurements of the optical density at 600 nm (OD_{600}). GST itself was applied as a control protein without any nuclease activity. The uncertainty of the measurements has not been plotted to simplify the diagram The average error was considered to be ±0.03 OD_{600} units. **c** The sodium dodecyl sulfate–polyacrylamide gel electrophoresis of the expressed proteins. (GST-NColE7′ is a toxic variant of NColE7—not detailed here) **d** The structure of NColE7 [Protein Data Bank (PDB) ID 1MZ8] in complex with a phosphate ion. Among the N-terminal amino acids, R447 is the closest to the phosphate ion that is bridging it with the Zn^{2+} ion. The diagram was created with PyMOL [58]

inserted into the pGEX-6-P1 (GE Healthcare) vector between the *Eco*RI and *Xho*I restriction enzyme sites (underlined sequences). The inserted DNA sequences contained a C-terminal stop codon (in italic in the primer sequence). The plasmids encoding the mutant proteins with a GST affinity tag at the N-terminus were cloned in *E. coli* DH10B or Mach1 (Invitrogen) cells and then transformed into *E. coli* BL21 (DE3), spread on Luria–Bertani medium supplemented with 100 μg/ml ampicillin (LB/Amp) plates and colonies were grown overnight at 37 °C. A small amount (4 ml) of LB/Amp medium was inoculated with a single colony and incubated overnight at 37 °C with shaking at 300 rpm. For large-scale protein production, the small-scale overnight cultures were transferred to 250 ml LB/Amp medium and bacteria were grown at 37 °C. The protein expression was induced by adding isopropyl β-thiogalactoside (200 mg/ml) to a final concentration of 0.42 mM to the cultures at an optical density at 600 nm (OD_{600}) of 0.5–0.6. The shaking at 140 rpm was continued for 2–3 h, until OD_{600} increased to 0.9–1.0. Cells were sedimented by centrifugation at 4 °C and 5,000*g* for 10 min, then resuspended in phosphate-buffered saline (PBS; 1.4 M NaCl, 27 mM KCl, 100 mM Na_2HPO_4, 18 mM KH_2PO_4, pH 7.3). Pellets were disrupted by sonication and the debris was removed by centrifugation at 5,000*g* and 4 °C for 10 min. The supernatant and the resuspended aggregates were analysed by 12.5 % sodium dodecyl sulfate–polyacrylamide gel electrophoresis (SDS-PAGE). A significant amount of the desired protein was present in inclusion bodies. The GST-based affinity purification step was done only with the soluble fractions. The protein solutions were loaded onto a 4-ml glutathione Sepharose 4B affinity column (Amersham Biosciences). The column was washed with ice-cold PBS to remove unbound material and then the bound fusion proteins were eluted with 15 mM reduced glutathione dissolved in PBS, containing 0.1 % Triton X-100 non-ionic detergent. Following an SDS-PAGE analysis, the fractions containing the target protein were pooled. Before the cleavage of the GST fusion tag, the excess of reduced glutathione was removed by dialysis against PBS, applying 150 times dilution. For digestion 1 μl (2 U/μl) of PreScission protease (GE Healthcare) was added for each 100 μg of fusion protein. The solution was incubated at 5 °C for 4 h. Following cleavage, batch purification was applied to remove the GST moiety and the PreScission protease (siliconized tubes were used to prevent the resin from sticking to the walls of the tubes): the glutathione Sepharose 4B resin was incubated with the protein solution for 30 min at 4 °C with gentle rotation. The medium was sedimented by centrifugation at 500*g* for 5 min and the supernatant was carefully transferred to new tubes. The efficiency of cleavage was checked by 17.5 % SDS-PAGE. The concentration was estimated from the gel, by comparing the intensity of the protein band with the intensity of the standard low-range (14–97 kDa) protein marker (Bio-Rad) applied in known concentrations (i.e. 5, 10, 15 and 20 μl from a 100 ng/μl stock solution). The large-scale protein expression and purification procedure has been detailed elsewhere [43].

Electrospray ionization mass spectrometry

Mass spectrometry measurements were obtained with an LCT Premier (Waters) instrument equipped with a Nanoflow electrospray ionization source and a time-of-flight analyser. The instrument was operated in positive ion mode and was calibrated using 100 mg/ml CsI in 50 % 2-propanol in the *m/z* range from 600 to 12,000. Samples were sprayed from medium-sized Au/Pd-coated borosilicate glass capillary needles (Proxeon) loaded with 3 μl protein solution. The protein concentration was 10–20 μM in 100 mM ammonium acetate (Sigma) buffer. The desalting of the protein solution and buffer exchange to the volatile buffer was done using a Micro BioSpin chromatography column (Bio-Rad). The needle voltage was typically around 1,200 V, and a cone voltage of 50 V was applied, with the cone gas flow rate maintained at 20 l/h and the source temperature maintained at 50 °C. A stock solution of 100 μM zinc(acetate)$_2$ (Sigma) was used to titrate the 20 μM ΔN25-NColE7 protein solution. The recorded *m/z* data were deconvoluted using MassLynx^{TM} version 4.1 (Waters) equipped with the MaxEnt1 algorithm. The high charge states of the multiply charged spectrum, ranging from +10 to +17, were used to calculate the apparent mass.

Gel mobility shift assay

An approximately 400 bp double-stranded DNA (dsDNA) was used as the substrate for gel mobility shift assays, and 50–100 ng of this DNA was used for each assay. The protein-to-dsDNA molar ratio ranged between 0.5:1 and 50:1, the protein-to-Zn^{2+} molar ratio was 1:1, 50 mM tris(hydroxymethyl)aminomethane/HCl buffer, pH 7.4 or PBS was used, and the final concentration of NaCl was adjusted to 50 mM. The solutions also contained 5 % glycerol. The reaction mixtures were incubated for 20–40 min at room temperature and then loaded onto 1 % agarose gel and run at 30–50 V in a buffer of 44.5 mM tris(hydroxymethyl)aminomethane, 1 mM EDTA, 44.5 mM boric acid, pH 7.3. Finally, the gel was stained with ethidium bromide solution with a concentration of 0.5 μg/ml for 30 min, followed by washing several times with distilled water. The documentation was done using UV light (Printgraph—ATTO,

Tokyo, Japan—or UVIdoc—UVItec, Cambridge, UK—gel documentation systems) at 312 nm.

SRCD spectroscopy measurements

The SRCD spectra of the proteins were recorded at the SRCD facility at the CD1 beamline [44] on the storage ring ASTRID at the Institute for Storage Ring Facilities (ISA), University of Aarhus, Denmark. The instrument was calibrated against camphorsulfonic acid. All spectra were recorded with 1 nm steps and a dwell time of 3 s per step, using 100-μm quartz cells (SUPRASIL, Hellma, Germany) for the wavelength range of 175–350 nm. The proteins were dissolved in distilled water and the pH was adjusted with HCl and NaOH solutions. The protein concentrations ranged from 10 to 50 μM. The water baseline was subtracted from raw spectra.

Fluorimetry

The most popular fluorescent probes for Zn^{2+} ions in living organisms contain quinoline units, such as 6-methoxy-(8-*p*-toluenesulfonamido)quinoline and its derivatives. These coordinate to the Zn^{2+} ion by four nitrogen donor atoms in the bis complex as illustrated in Fig. S1, but the protonation state of the complex changes with pH [45]. The fluorofor used in this study was an acid derivative of 6-methoxy-(8-*p*-toluenesulfonamido)quinoline: 4-[([6-methoxy-2-methyl-8-quinolinyl]amino)sulfonyl]benzoic acid (TFLZn) test (Sigma-Aldrich). It is soluble in water and shows high Zn^{2+} ion selectivity compared with other cations. Its affinity for Zn^{2+} ions is high enough to bind the free biological metal ion ($K_D \approx 20$ μM), but is not high enough to extract Zn^{2+} coordinated in proteins. TFLZn shows little fluorescence in the absence of Zn^{2+}. Upon formation of the bis complex, a 100-fold increase in intensity is experienced. The maxima of the excitation and emission spectra are at 360 and 498 nm, respectively.

The measurements were performed with a Hitachi F-4500 fluorescence spectrometer in a 1 cm × 1 cm path length quartz cell. The solutions were irradiated in the wavelength range between 340 and 420 nm, and the emission spectrum was recorded between 400 and 600 nm. The TFLZn concentration was adjusted to 5 μM in all cases, and mutant proteins were added in a concentration range between 0.37 and 4.8 μM. The Zn^{2+} concentration ranged from 1.2 to 27.5 μM, the EDTA concentration ranged from 1.2 to 30 μM and the DNA concentration (a 10 bp DNA string was considered to be a binding unit) ranged from 0.5 to 1.5 μM in the titration experiments.

Calculations

The initial conformation of NColE7 and the shortened mutants was taken from the Protein Data Bank (PDB) structure 1M08 [6]. This structure has a methionine (M446) instead of K446 at the N-terminus. The wild-type NColE7 calculations were done from the M446K mutant of the original PDB structure. All proteins had unprotected termini (i.e. NH_3^+ and COO^- groups).

Molecular dynamics calculations were performed with GROMACS 4.05 [46, 47], with the Gromos 53a6 [48] force field. The ionizable residues were charged according to the default pK_a values at pH 7.2, as no reason was found to alter the default pK_a values with use of propKa 3.0 [49]. The protein was placed in a cubic box with an edge size of approximately 8 nm, and was solvated by the explicit extended simple point charge (SPC/E) water model. About 16,000 equilibrated water molecules were needed to fill the box, which was neutralized owing to the positive charge of the protein by Cl^- ions replacing water molecules at the most positive parts of the box using GENION. Energy minimization was conducted using the steepest descent method. We performed 200 ps position-restrained dynamics simulations in the NVT ensemble to equilibrate the system (solvate and generate initial velocities with a Maxwell distribution) including explicit water molecules. We performed 20 ns productive molecular dynamics simulations in the NPT ensemble with periodic box conditions with integration steps of 2 fs. The temperature was set to 300 K and isotropic Berendsen P coupling and T coupling was used. For Coulomb interactions, the particle mesh Ewald method was applied with 0.9 nm electrostatic and 1.6 nm van der Waals interaction cut-offs, and the dielectric constant was set to 1.0. The constraint algorithm LINCS was used. Trajectories were analysed starting at 500 ps.

Semiempirical quantum chemical computations were performed using MOPAC2009 [50] with the PM6 method [51, 52]. Localized molecular orbitals were applied using the MOZYME [53] model implemented in MOPAC2009. The solvation was considered by the conductor-like screening model method [54] with a dielectric constant of 78.4. The geometry optimization was done by the quasi-Newton limited-memory Broyden–Fletcher–Goldfarb–Shanno method after the initial minimization of the hydrogen positions. A gradient norm of approximately 2–3 kcal/mol was achieved, and the heat of formation became essentially stationary.

Results and discussion

Cytotoxic effect of the mutant proteins

To study the necessity of the N-terminal end of the NColE7 protein for its activity, first the genes of the truncated mutants were constructed and inserted into a pGEX-6P-1 vector. The ΔN4-NColE7 and ΔN25-NColE7 proteins were designed to delete four and 25 N-terminal amino acids